nature genetics

LETTERS

https://doi.org/10.1038/s41588-020-0623-4

Check for updates

Cas9 activates the p53 pathway and selects for p53-inactivating mutations

Oana M. Enache[1,9], Veronica Rendo[2,9], Mai Abdusamad[1], Daniel Lam[1], Desiree Davison[1], Sangita Pal[2], Naomi Currimjee[2], Julian Hess[1], Sasha Pantel[3], Anwesha Nag[4], Aaron R. Thorner[4], John G. Doench[3], Francisca Vazquez[1], Rameen Beroukhim[1,2,5], Todd R. Golub[1,5,6,7] and Uri Ben-David[1,8] ✉

Cas9 is commonly introduced into cell lines to enable CRISPR–Cas9-mediated genome editing. Here, we studied the genetic and transcriptional consequences of Cas9 expression itself. Gene expression profiling of 165 pairs of human cancer cell lines and their Cas9-expressing derivatives revealed upregulation of the p53 pathway upon introduction of Cas9, specifically in wild-type *TP53* (*TP53*-WT) cell lines. This was confirmed at the messenger RNA and protein levels. Moreover, elevated levels of DNA repair were observed in Cas9-expressing cell lines. Genetic characterization of 42 cell line pairs showed that introduction of Cas9 can lead to the emergence and expansion of p53-inactivating mutations. This was confirmed by competition experiments in isogenic *TP53*-WT and *TP53*-null (*TP53*$^{-/-}$) cell lines. Lastly, Cas9 was less active in *TP53*-WT than in *TP53*-mutant cell lines, and Cas9-induced p53 pathway activation affected cellular sensitivity to both genetic and chemical perturbations. These findings may have broad implications for the proper use of CRISPR–Cas9-mediated genome editing.

Neutral genetic manipulations can lead to genetic and transcriptional diversification of cell lines, most likely due to culture bottlenecks associated with such manipulations[1,2]. However, it is currently unknown whether introduction of specific 'neutral' genes can select for the acquisition or expansion of specific genetic alterations. Of particular interest is Cas9 (CRISPR-associated protein 9), which is commonly introduced into cell lines to facilitate genome editing[3–5]. Whether Cas9 expression itself is sufficient to elicit cellular stress responses remains unknown (Supplementary Note 1).

To test whether Cas9-expressing cell lines (hereafter referred to as Cas9 lines) differ in any systematic way from their parental lines (hereafter referred to as WT lines) we performed expression profiling of 165 pairs of WT and Cas9 lines, using the L1000 assay[6] (Supplementary Data 1). Each line was profiled in 16 technical replicates, and global expression profiles were then compared between WT and Cas9 lines to characterize a Cas9 transcriptional signature (Methods). As expected, the expression patterns of all Cas9 lines were similar to those of their parental WT lines, and all of the pairs (165 out of 165) clustered together in an unsupervised hierarchical clustering (Extended Data Fig. 1a). However, significant transcriptional differences were observed between Cas9 and WT lines. The pairwise transcriptional difference between the groups significantly exceeded the transcriptional variation observed when comparing replicates within each group (Extended Data Fig. 1b). A median of 87 genes (range, 2–1,650) were differentially expressed by at least twofold between pairs ($P<0.05$; $q<0.05$; Fig. 1a, Table 1 and Supplementary Note 2). Gene set enrichment analysis (GSEA)[7,8] revealed that differentially expressed genes often converged on MSigDB Hallmark gene sets (Fig. 1b). Importantly, the transcriptional effect of Cas9 was stronger than that observed in a similar analysis of lines expressing empty or reporter vectors ($P=0.001$; Fig. 1b and Extended Data Fig. 1b), and was not merely a reflection of Cas9 infectability (Extended Data Fig. 1c).

Next, we asked whether any specific cellular pathways were consistently activated or suppressed in Cas9 lines compared to WT lines. GSEA revealed a significant activation ($P<0.05$; $q<0.05$) of the p53 pathway in 25 (15.2%) of the pairs. Importantly, this activation was enriched in *TP53*-WT lines compared to lines harboring an inactivating *TP53* mutation (33% of the *TP53*-WT pairs versus 9% of the *TP53*-mutant pairs, $P=0.0008$; Extended Data Fig. 1d). When individual pairwise comparisons of Cas9 and WT lines were aggregated to generate a universal signature of Cas9 activation across lines (Methods), activation of the p53 pathway was one of the two most significantly activated pathways in the Cas9 lines (together with NF-κB signaling). This was significantly enriched in *TP53*-WT lines, and was not observed in lines expressing empty or reporter vectors (Fig. 1c, Extended Data Fig. 1e–g Supplementary Data 2 and Supplementary Note 3).

Immunoblotting confirmed p53 pathway activation upon Cas9 introduction into *TP53*-WT cells. Modestly elevated levels of p53 and/or p21 protein expression were observed in seven out of eight independent Cas9 introduction experiments across five *TP53*-WT lines ($P=0.027$ and $P=0.024$ for p53 and p21, respectively; Fig. 1d,e), but was not detected in four independent Cas9 introduction experiments across four *TP53*-mutant lines ($P=0.01$ for the comparison between groups; Fig. 1d,e). Analysis by reverse-transcription quantitative PCR (RT–qPCR) confirmed that Cas9 lines—but not lines expressing GFP, luciferase or a DNA barcode—exhibited elevated mRNA levels of multiple p53 transcriptional targets (Fig. 1f, Extended Data Fig. 2a,b and Table 1).

To further rule out the possibility that the observed p53 activation is merely a consequence of viral transduction, or that it would occur following the overexpression of any gene, we performed the following experiments. First, we transfected the *TP53*-WT lines MCF7 and HCT116 with either Cas9, GFP or a backbone-matched

[1]Cancer Program, Broad Institute of Harvard and MIT, Cambridge, MA, USA. [2]Department of Cancer Biology, Dana-Farber Cancer Institute, Boston, MA, USA. [3]Genetic Perturbation Platform, Broad Institute of Harvard and MIT, Cambridge, MA, USA. [4]Center for Cancer Genome Discovery, Dana-Farber Cancer Institute, Boston, MA, USA. [5]Harvard Medical School, Boston, MA, USA. [6]Howard Hughes Medical Institute, Chevy Chase, MD, USA. [7]Department of Pediatric Oncology, Dana-Farber Cancer Institute, Boston, MA, USA. [8]Department of Human Molecular Genetics & Biochemistry, Faculty of Medicine, Tel Aviv University, Tel Aviv, Israel. [9]These authors contributed equally: Oana M. Enache, Veronica Rendo. ✉e-mail: ubendavid@tauex.tau.ac.il

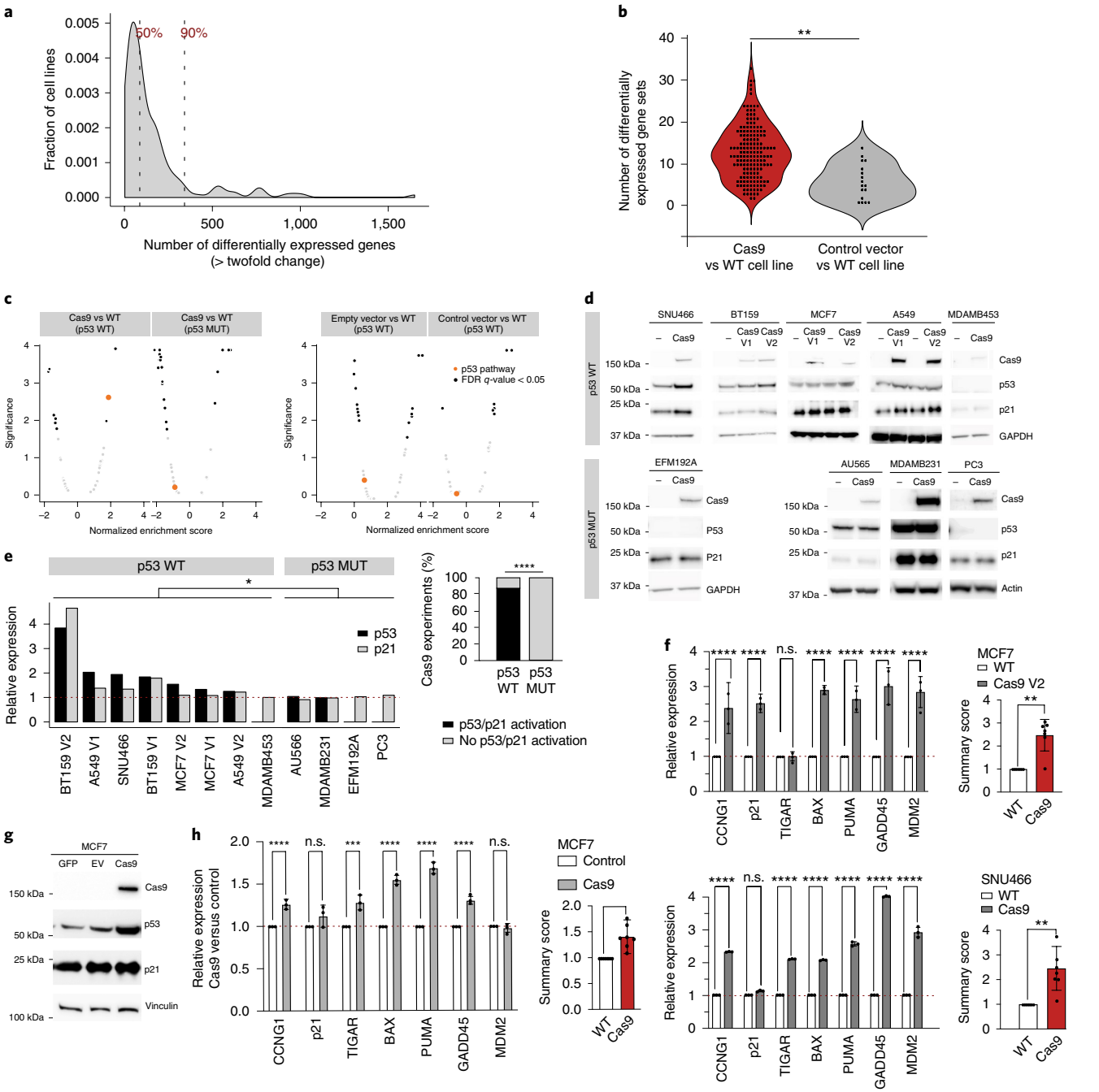

Fig. 1 | Cas9 introduction can activate the p53 pathway. a, The number of differentially expressed genes (fold change ≥ 2) across 165 Cas9 versus WT transcriptional signatures. Dashed vertical lines highlight the median (87 genes) and the 90th percentile (389 genes). **b**, The number of MSigDB Hallmark biological pathways that are significantly enriched (GSEA enrichment score with multiple hypotheses correction; FDR, $q < 0.05$) following the introduction of Cas9 (red) or empty or control vectors (gray). $^{**}P = 0.001$, two-sided Kolmogorov–Smirnov test. Data points represent cell line pairs. **c**, The degree and significance of modulation of the 50 MSigDB Hallmark biological pathways, following the introduction of empty vectors, reporter vectors or Cas9 into *TP53*-WT cell lines, and the introduction of Cas9 into *TP53*-mutant cell lines. Black, significantly enriched (GSEA enrichment score with multiple hypotheses correction; FDR, $q < 0.05$) pathways. Orange, the p53 pathway. Each plot represents the results of one Aggregate expression signature (Methods). **d**, Protein levels of Cas9, p53, p21 and a housekeeping protein in eight *TP53*-WT lines and four *TP53*-mutant lines before and after Cas9 introduction. Representative results of three independent experiments are shown. **e**, Left, western blot quantification. Each bar represents a western blot shown in **d**. $^{*}P = 0.027$ and $P = 0.024$ for p53 and p21, respectively; one-tailed Wilcoxon rank test. Right, the fraction of lines that activated p53 or p21 in response to Cas9 introduction. $^{*}P = 0.01$, one-tailed Fisher's exact test. **f**, Left, confirmation of p53 pathway activation in MCF7 and SNU466 by RT-qPCR analysis of seven p53 transcriptional targets. $^{****}P < 0.0001$, one-tailed *t*-test. Right, the average activation of p53 transcriptional targets. $^{**}P < 0.01$, two-sided one-sample *t*-test. n.s., not significant. **g**, Protein levels of Cas9, p53, p21 and a housekeeping protein in MCF7 cells transfected with GFP, Cas9 or a backbone-matched empty vector (EV). Representative results of three independent experiments are shown. **h**, Left, confirmation of p53 activation in MCF7 cells transfected with Cas9 by RT-qPCR analysis of seven p53 transcriptional targets. Shown is the relative activation in cells transfected with Cas9 compared to cells transfected with control vectors. $^{***}P = 0.0002$, $^{****}P < 0.0001$, one-tailed *t* test. Right, the average activation of p53 transcriptional targets. $^{*}P < 0.05$, two-sided one-sample *t*-test. For all bar plots, the data values are the means of the seven targets; error bars, s.d.

Table 1 | Summary table

Type of profiling	p53 status	No. of unique cell lines	% cell lines with > 100 genes deregulated (>2×)	% cell lines with p53 pathway activation	% cell lines with emergence or expansion of a p53 mutation (ΔAF > 0.05)
Gene expression	WT	43	44.2%	32.6%	NA
	Mutant	122	43.4%	9.1%	NA
Western blot + RT-qPCR	WT	5	NA	80%	NA
	Mutant	4	NA	0%	NA
Targeted DNA sequencing	WT	14	NA	NA	14.3%
	Mutant	26	NA	NA	7.7%

The number of *TP53*-WT and *TP53*-mutant cell lines that were included in each experimental assay, the percentage of cell lines with > 100 genes deregulated by > twofold change, the percentage of cell lines with significant activation of the p53 pathway, and the percentage of cell lines with emergence or expansion of a functional *TP53* mutation (ΔAF > 0.05). NA, not applicable.

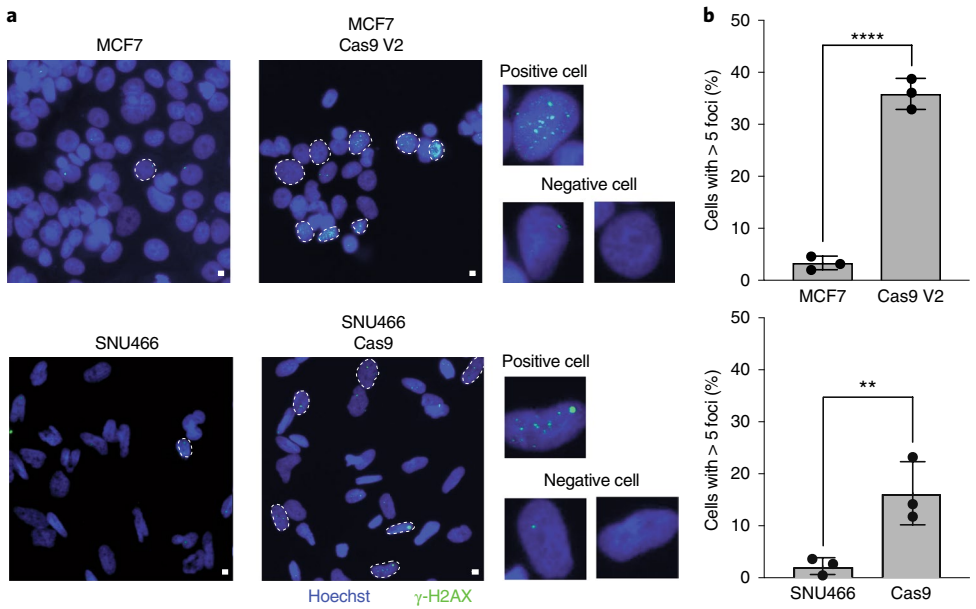

Fig. 2 | Cas9 introduction is associated with elevated DNA damage. a, Fluorescent microscopy images of γH2AX foci (green) and DAPI (blue) in WT and Cas9 MCF7 and SNU466 cells. Cells with more than 5 foci have been marked in white. Scale bars, 10 µm. Representative images of three independent experiments are shown. **b**, Quantification of γH2AX foci from three independent repeats; $n = 841$ and $n = 1{,}056$ for WT and Cas9 MCF7 cells, respectively; $n = 752$ and $n = 810$ for WT and Cas9 SNU466 cells, respectively. $P < 0.0001$ and $P = 0.009$, for MCF7 and SNU466, respectively; one-tailed *t* test. Data values represent the means, error bars correspond to s.d.

empty vector. In MCF7 cells, p53 activation was significantly stronger in the Cas9-expressing cells (Fig. 1g,h). In HCT116 cells, we did not observe a significant difference in p53 pathway activity between the different transfections (Extended Data Fig. 2c); however, when we transduced isogenic *TP53*-WT and *TP53*-null HCT116 lines[9] with viruses carrying either Cas9 or a backbone-matched empty vector, p53 activation was significantly stronger upon Cas9 transduction (and was specific to the *TP53*-WT cells; Extended Data Fig. 2d,e). Together, these findings demonstrate that Cas9-induced p53 activation cannot be explained by technical noise, by the effect of viral transduction, or by a general selection bottleneck.

The well-established role of p53 in response to DNA damage makes its activation in the context of Cas9 expression particularly interesting (Supplementary Note 4)[10–13]. Notably, NF-κB signaling was the other most significantly activated pathway following Cas9 introduction specifically (Supplementary Data 2). Both p53 and NF-κB are major regulators of the transcriptional response to DNA damage[14,15], alluding to a potential involvement of DNA damage in the observed p53 response. Indeed, a DNA repair transcriptional signature[7] was positively enriched following Cas9 introduction in 32 (19.4%) of the line pairs, in both *TP53*-WT and *TP53*-mutant lines ($P = 0.07$; Extended Data Fig. 3a). Immunofluorescence of three pairs confirmed that expression of Cas9 increased the number of DNA double-strand breaks, as measured by γH2AX foci ($P < 0.0001$; Fig. 2a,b and Extended Data Fig. 3b,c).

Activation of the p53 pathway following Cas9 introduction suggests that p53 activity is a barrier that cells need to overcome to stably express Cas9. Cas9 introduction might therefore select for p53-inactivating mutations. To test this hypothesis, we characterized point mutations of 447 cancer genes in 42 pairs of WT and Cas9 lines, using deep (283×) targeted exon sequencing[16] (Methods and Supplementary Data 3). The mutational landscapes of Cas9 lines were all highly similar to those of their parental counterparts, as expected (Extended Data Fig. 4a,b). When considering only non-synonymous single-nucleotide variants (SNVs) and indels affecting the coding sequence, an average of 2.6 mutations

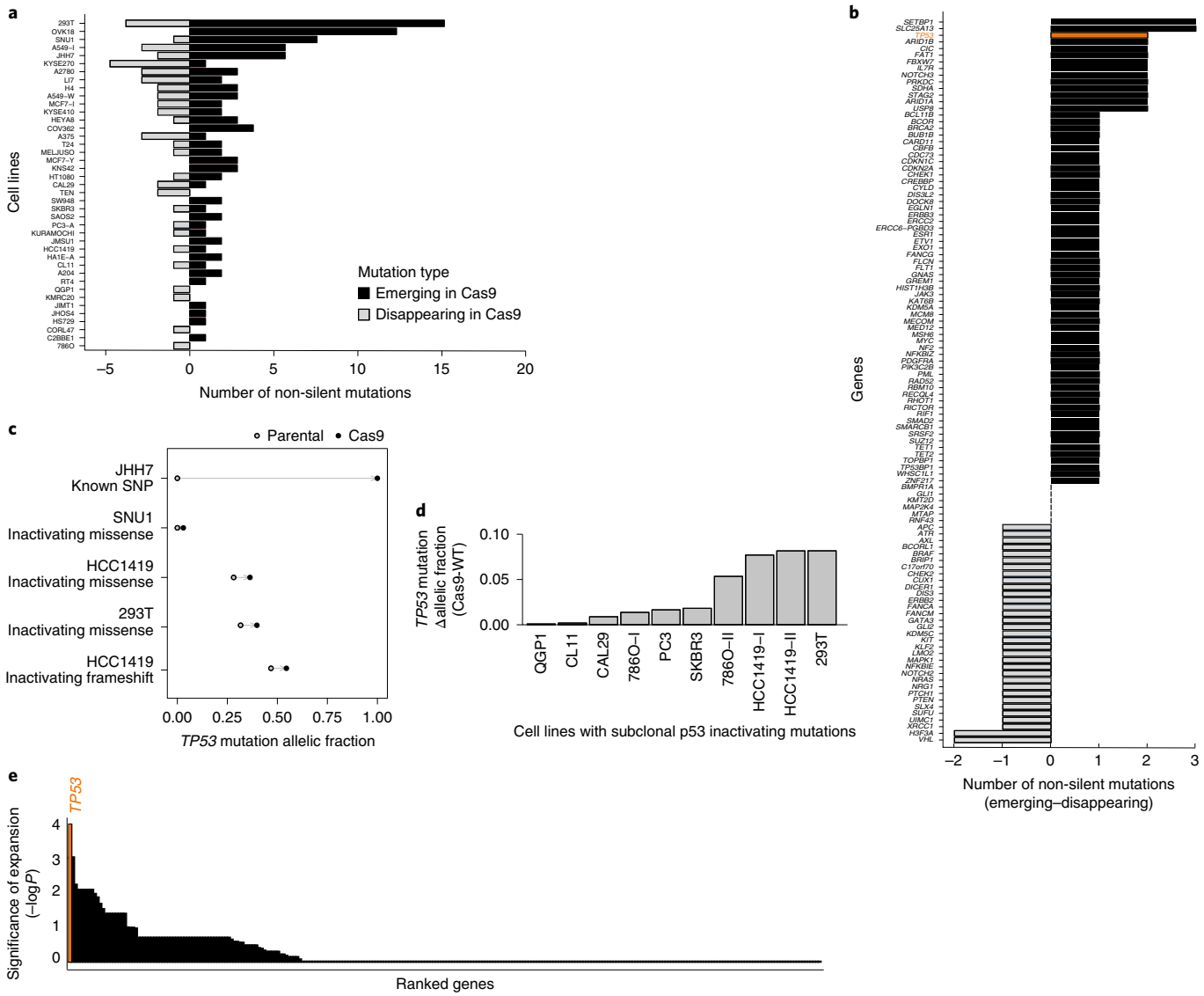

Fig. 3 | Cas9 introduction selects for inactivating *TP53* mutations. a, The number of non-silent mutations that differ between the profiled Cas9 lines and their matched WT lines (that is, mutations detected in either the parental or the Cas9 line, but not in both). Emerging mutations are shown in black, disappearing mutations in gray. $^*P=0.01$, one-tailed paired *t*-test. **b**, Cancer-related genes ranked by their tendency to acquire non-silent mutations in the Cas9 lines. *TP53* is highlighted in orange, and is among the top 4% of genes to acquire new mutations upon Cas9 introduction (out of 128 genes with a non-silent mutation present). **c**, Changes in the allelic fraction of five non-silent *TP53* mutations in four independent cell line pairs. Two of the mutations could not be detected in the parental WT line at all, and the other three were detected at lower allelic fractions. **d**, Changes in the allelic fraction of ten pre-existing subclonal inactivating *TP53* mutations across eight cell line pairs. $^*P=0.005$, one-tailed paired *t*-test. **e**, Cancer genes ranked by the significance (based on two-tailed one-sample Wilcoxon rank test) of non-silent subclonal mutation expansion following Cas9 introduction. *TP53* is highlighted in orange, and ranks first in this analysis (out of 276 genes).

were detected in Cas9 lines but not in their parental WT lines, and an average of 1.3 mutations were detected in WT lines but not in their derivative Cas9 lines (Fig. 3a). This means that Cas9 lines tend to acquire new mutations more often than they tend to lose them ($P=0.003$). On average, approximately 4.5 non-silent mutations in bona fide cancer-related genes separated Cas9 lines from their parental WT lines (Fig. 2a, Extended Data Fig. 4c and Supplementary Note 5).

TP53 was among the top 4% of genes in its tendency to acquire new mutations upon Cas9 introduction (Fig. 3b). Non-silent *TP53* mutations emerged in the Cas9 line of 2 out of the 42 examined pairs, SNU1 and JHH7, and significantly expanded in two additional lines, 293T and HCC1419 (which had two such mutations, both of which expanded; $P=0.008$ and $P=0.047$; Fig. 3c and Table 1). For JHH7, the mutation was not detected in the parental WT line, but became clonally homozygous (with an allele frequency (AF) of 1) in the Cas9 line (Fig. 3c, Extended Data Fig. 4d and Supplementary Note 6). In three of these four lines (SNU1, HCC1419 and 293T), the mutations that emerged or expanded in the Cas9 line were bona fide inactivating mutations[17]. Importantly, changes in the opposite direction (that is, detection of a non-silent *TP53* mutation only in the WT line and not in its Cas9 derivative) were never observed (Extended Data Fig. 4e). Moreover, we identified a total of ten pre-existing subclonal inactivating *TP53* mutations in eight lines, and found a mild but significant ($P=0.005$) tendency towards expansion of these mutations in the Cas9 lines (Fig. 3d). Notably, we did not detect a non-silent *TP53* mutation emerging or expanding following lentiviral transduction of a reporter or a DNA

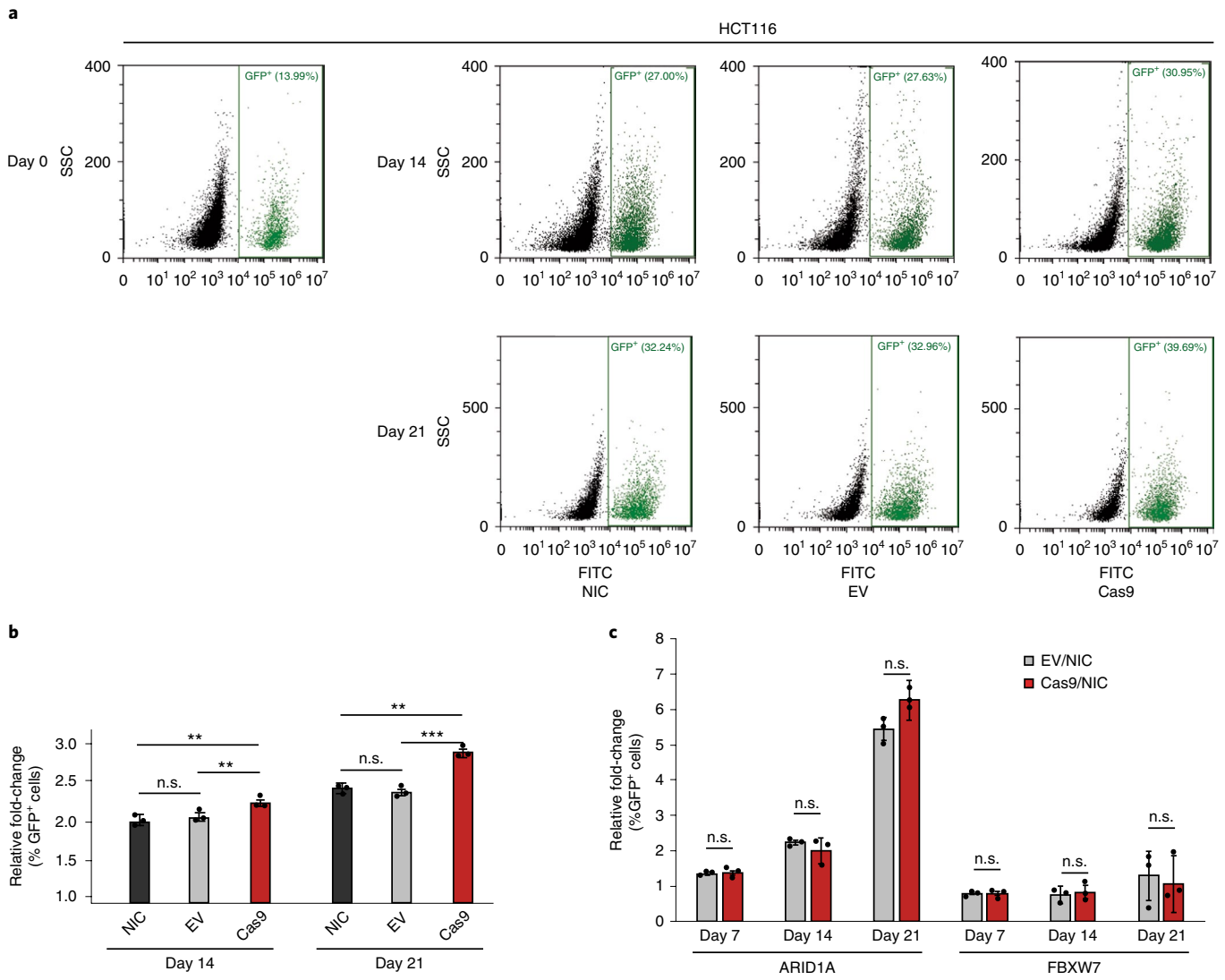

Fig. 4 | Expansion of inactivating *TP53* mutations is accelerated by Cas9 in a cell competition assay. a, Representative flow cytometry scatter plots, gated by GFP expression. The proportion of HCT116 *TP53*-null/GFP$^+$ was quantified at day 0, day 14 and day 21 after infection with backbone-matched empty vector (EV) or Cas9 vector, or without infection at all (no-infection control, NIC). Representative results of three independent experiments are shown. **b**, Quantification of the flow cytometry experiments shown in **a**. $n=3$ cell culture replicates per condition. At day 14 and day 21, the proportion of *TP53*-null cells in the population is significantly higher in cells infected with Cas9 compared to the EV and NIC. $P=0.003$ and $P=0.001$ for the comparisons of NIC versus Cas9 and EV versus Cas9 at day 14, respectively; $P=0.001$ and $P=6.4\times10^{-5}$ for the comparisons of NIC versus Cas9 and EV versus Cas9 at day 21, respectively; two-tailed *t*-test. Data values represent the means of three cell culture replicates for each condition at each time point, with error bars corresponding to s.d. **c**, Comparison of the cell competition experiments in *ARID1A*-null and *FBXW7*-null HCT116 cells. For *ARID1A*, $P=0.65$ and $P=0.34$ and $P=0.1$ for the comparisons of day 7, day 14 and day 21, respectively; for *FBXW7*, $P=0.94$, $P=0.79$ and $P=0.71$ for the comparisons of day 7, day 14 and day 21, respectively; two-tailed *t*-test. Data values represent the means of three replicates for each condition at each time point, error bars correspond to s.d.

barcode, in nine independent experiments across three *TP53*-WT lines (Extended Data Fig. 4f), further supporting the Cas9 specificity of the phenomenon.

To address whether the significant tendency of p53-inactivating mutations to expand following Cas9 introduction is unique to this gene, or common to all or other tumor suppressor genes, we analyzed the AF of all subclonal non-silent mutations across all 447 genes included in our sequencing panel. The tendency of mutated subclones to expand (increased AF) was greater for *TP53* than for any other gene (Fig. 3e and Supplementary Data 4). Next, we compared the relative abundance of emerging silent vs. non-silent mutations in *TP53* and all other genes, to ask whether *TP53* is significantly enriched for functional non-silent mutations in comparison to other tumor suppressor genes. The ratio of silent to non-silent emerging mutations in *TP53* was ranked number 5 (in the top ~1%) of all genes (Extended Data Fig. 4g, Supplementary Data 4 and Supplementary Note 7).

Next, we performed a cell competition assay with isogenic HCT116 lines: enhanced green fluorescent protein (eGFP)-labeled *TP53*-null cells were transduced with viruses carrying either Cas9 or a backbone-matched empty vector, mixed with their isogenic *TP53*-WT cells (1:8 ratio), and their proportion in the population was monitored over time by flow cytometry. As expected, the proportion of *TP53*-null cells gradually increased with time. Importantly, this expansion was faster when cells were infected with Cas9 compared to the empty vector and no-infection

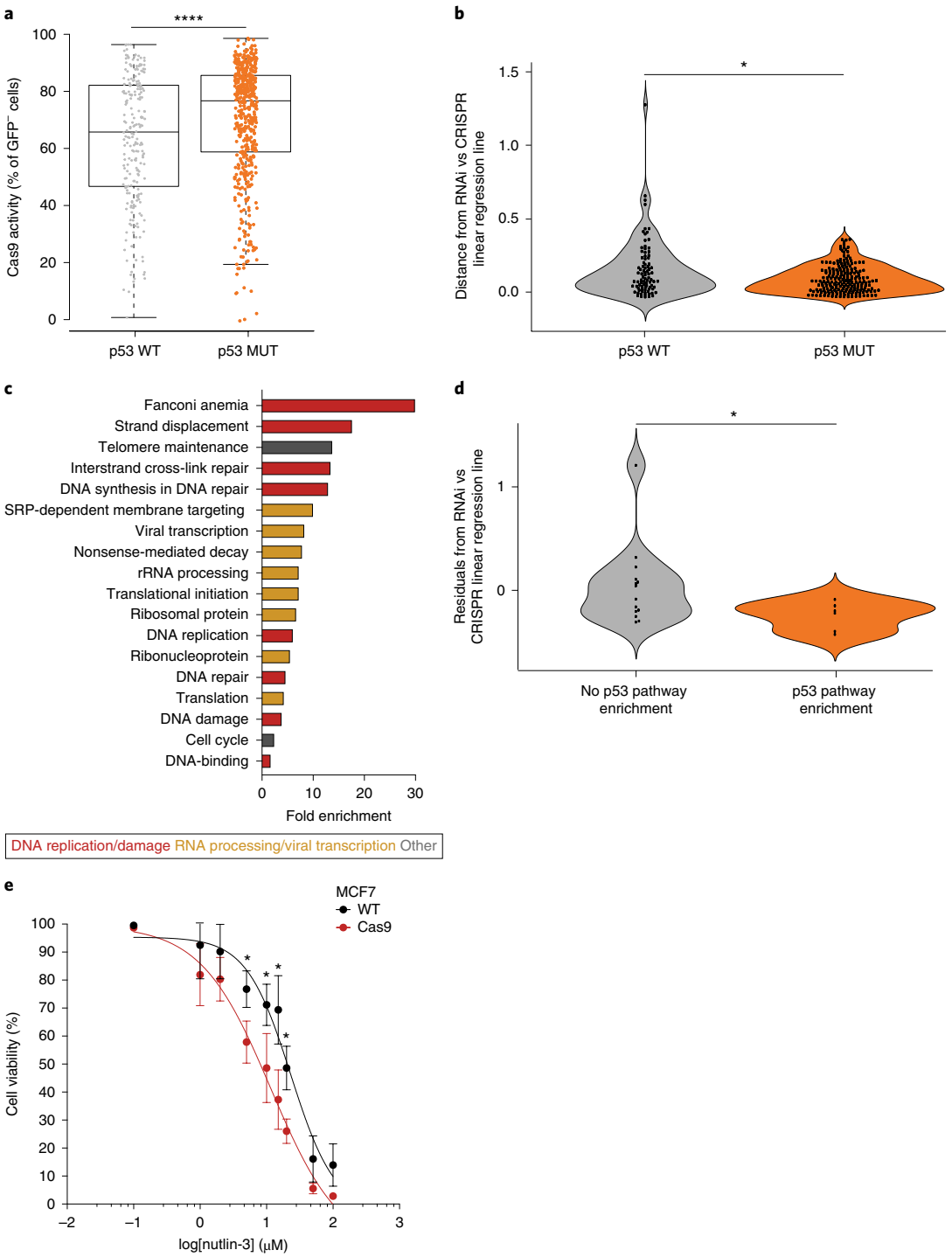

Fig. 5 | Cas9-induced p53 activation can functionally affect genetic and chemical perturbation assays. a, Comparison of Cas9 activity between 216 *TP53*-WT and 482 *TP53*-null cell lines, using an eGFP-based Cas9 activity assay[20]. The higher the fraction of GFP-negative cells, the higher the level of Cas9 activity. Bar, median; box, 25th and 75th percentile; whiskers, 1.5 times the interquartile range of the lower and upper quartiles; circles, individual cell lines. *$P = 2.7 \times 10^{-5}$, one-tailed *t*-test. **b**, Comparison of the concordance between CRISPR and RNAi gene perturbation screens in 86 *TP53*-WT and 207 *TP53*-mutant cell lines. Shown is the absolute distance from the CRISPR–RNAi linear regression line: the higher the distance the less concordant the CRISPR and RNAi screens are. *$P = 0.022$, one-tailed Wilcoxon rank test. Data points represent cell lines. **c**, Gene sets that are significantly enriched (DAVID functional annotation analysis with multiple hypotheses correction; $P < 0.01$, $q < 0.25$) in the list of genes that are selectively essential in 86 *TP53*-WT cell lines in the CRISPR, but not in the RNAi genetic screen. Gene sets are colored by their functional category. **d**, Comparison of the concordance between CRISPR and RNAi gene perturbation screens in 20 *TP53*-WT cell lines that exhibited p53 pathway activation in L1000 Cas9 versus WT signatures and those that did not. Shown is the distance from the CRISPR–RNAi regression line: negative values represent a stronger proliferation effect of p53 inhibition in CRISPR versus RNAi screen. *$P = 0.02$, one-tailed *t*-test. Data points represent cell lines. **e**, Dose response curves of the response of parental and Cas9-expressing MCF7 cells to the MDM2 inhibitor nutlin-3. *$P = 0.029$, $P = 0.01$, $P = 0.0004$, and $P = 0.0099$ for 5 μM, 10 μM, 15 μM and 20 μM, respectively, two-way ANOVA. Data values represent the means of three cell culture replicates for each condition at each time point, error bars correspond to s.d.

controls ($P = 0.0013$ and $P = 6.3 \times 10^{-5}$, respectively; Fig. 4a,b), indicating that Cas9 increases the adaptive value of p53 inactivation. We repeated the cell competition experiment with two additional tumor suppressor genes, *ARID1A* and *FBXW7* (Supplementary Note 8). In contrast to the Cas9-induced expansion of the *TP53*-null cells, *ARID1A*-null and *FBXW7*-null cells did not expand more quickly following Cas9 introduction compared to the empty vector controls (Fig. 4c). These data demonstrate that Cas9 expression selects specifically for p53-inactivating mutations, rather than for mutations in other tumor suppressor genes.

Based on all previous findings, we predicted that Cas9 activity in *TP53*-WT lines would be lower, on average, than that in *TP53*-mutant lines. We therefore compared Cas9 activity between 216 *TP53*-WT and 482 *TP53*-mutant lines, using a quantitative functional assay of Cas9 activity[18]. Indeed, Cas9 activity was significantly lower in *TP53*-WT lines ($P = 3.1 \times 10^{-5}$; Fig. 5a and Supplementary Data 5), confirming that p53 activity jeopardizes the efficient expression of Cas9.

To address whether the phenomenon described in this study has affected previous CRISPR–Cas9 screens, we compared the CRISPR–Cas9 and RNA interference (RNAi) genetic perturbation screens of the Broad Institute (Methods). The concordance in genetic dependencies between the CRISPR–Cas9 and the RNAi data sets was significantly lower in *TP53*-WT lines ($P = 0.022$; Fig. 5b). Next, we performed a functional annotation enrichment analysis on the list of genes that were more essential in the *TP53*-WT cells in the CRISPR–Cas9 screens, but not in the RNAi screens. This list was significantly enriched for genes related to two major functional categories: DNA replication and DNA damage repair, and RNA processing and viral transcription (Fig. 5c and Supplementary Data 6). This suggests that Cas9-induced DNA damage in *TP53*-WT cells increased the dependency on functional DNA repair machinery, consistent with a similar recent analysis[19]. Finally, we compared the dependency on *TP53* itself between *TP53*-WT lines in which p53 pathway activation was identified and *TP53*-WT lines in which such activation was not observed. The proliferation effect of *TP53* CRISPR–Cas9 knockout (relative to *TP53* RNAi knockdown) was significantly stronger in lines with Cas9-induced p53 pathway activation ($P = 0.02$; Fig. 5d). Together, these findings demonstrate that the phenomenon described here has indeed affected previous CRISPR–Cas9 screens.

To further test the functional implications of Cas9-induced p53 activation, we compared the response of parental and Cas9-expressing MCF7 cells to the MDM2 inhibitor nutlin-3. We found a modest but significant increase in drug sensitivity in the Cas9-expressing cells (Fig. 5e), consistent with our other findings. We conclude that Cas9-induced p53 activation can affect both genetic and chemical perturbation assays.

In summary, we found that Cas9 expression can elicit activation of the p53 pathway when introduced into human cell lines, leading to the emergence or expansion of inactivating *TP53* mutations ($\Delta AF > 0.05$) in approximately 10% of cases (Table 1). Our findings suggest that Cas9-induced DNA damage may underlie p53 activation, but the molecular mechanisms that lead to this response, as well as those that mitigate it to allow Cas9 tolerance in the absence of genetic selection, remain to be elucidated. Although we have not ruled out that some of the observed p53 activation could be attributed to the viral transduction itself[20,21], and that the presence of a sgRNA could exacerbate p53 activation further[10–12], our findings demonstrate Cas9-specific p53 activation. This p53 activation, albeit mild, is persistent and seems to be sufficient to select for p53-inactivating mutations.

We propose that it is therefore important to carefully investigate p53 status following the introduction of Cas9 into *TP53*-WT cells, as it may have implications for the interpretation of genetic and chemical CRISPR–Cas9-based screens, as well as for additional applications of the CRISPR–Cas9 technology (Supplementary Note 9 and Extended Data Fig. 5). A recent study suggested that CRISPR-induced p53 activation could be overcome by transient p53 silencing[12]. Our findings suggest that cells may overcome such p53 activation in another way—by selecting for p53-inactivating mutations—which could have long-term irreversible consequences. Further investigation is required to determine the potential physiological relevance of these findings for CRISPR–Cas9-based therapeutics.

Online content

Any methods, additional references, Nature Research reporting summaries, source data, extended data, supplementary information, acknowledgements, peer review information; details of author contributions and competing interests; and statements of data and code availability are available at https://doi.org/10.1038/s41588-020-0623-4.

Received: 7 September 2019; Accepted: 3 April 2020;

References

1. Ben-David, U., Beroukhim, R. & Golub, T. R. Genomic evolution of cancer models: perils and opportunities. *Nat. Rev. Cancer* **19**, 97–109 (2019).
2. Ben-David, U. et al. Genetic and transcriptional evolution alters cancer cell line drug response. *Nature* **560**, 325–330 (2018).
3. Cong, L. et al. Multiplex genome engineering using CRISPR/Cas systems. *Science* **339**, 819–823 (2013).
4. Jinek, M. et al. RNA-programmed genome editing in human cells. *eLife* **2**, e00471 (2013).
5. Mali, P. et al. RNA-guided human genome engineering via Cas9. *Science* **339**, 823–826 (2013).
6. Subramanian, A. et al. A next generation connectivity map: L1000 platform and the first 1,000,000 profiles. *Cell* **171**, 1437–1452 e17 (2017).
7. Liberzon, A. et al. The Molecular Signatures Database (MSigDB) hallmark gene set collection. *Cell Syst.* **1**, 417–425 (2015).
8. Subramanian, A. et al. Gene set enrichment analysis: a knowledge-based approach for interpreting genome-wide expression profiles. *Proc. Natl Acad. Sci. USA* **102**, 15545–15550 (2005).
9. Bunz, F. *et al*. Requirement for p53 and p21 to sustain G2 arrest after DNA damage. *Science* **282**, 1497–1501 (1998).
10. Haapaniemi, E., Botla, S., Persson, J., Schmierer, B. & Taipale, J. CRISPR–Cas9 genome editing induces a p53-mediated DNA damage response. *Nat. Med.* **24**, 927–930 (2018).
11. Ihry, R. J. et al. p53 inhibits CRISPR–Cas9 engineering in human pluripotent stem cells. *Nat. Med.* **24**, 939–946 (2018).
12. Schiroli, G. et al. Precise gene editing preserves hematopoietic stem cell function following transient p53-mediated DNA damage response. *Cell Stem Cell* **24**, 551–565.e8 (2019).
13. Wu, Y. et al. Highly efficient therapeutic gene editing of human hematopoietic stem cells. *Nat. Med.* **25**, 776–783 (2019).
14. Elkon, R. et al. Dissection of a DNA-damage-induced transcriptional network using a combination of microarrays, RNA interference and computational promoter analysis. *Genome Biol.* **6**, R43 (2005).
15. Wang, W., Mani, A. M. & Wu, Z. H. DNA damage-induced nuclear factor-kappa B activation and its roles in cancer progression. *J. Cancer Metastasis Treat.* **3**, 45–59 (2017).
16. Sholl, L. M. et al. Institutional implementation of clinical tumor profiling on an unselected cancer population. *JCI Insight* **1**, e87062 (2016).
17. Giacomelli, A. O. et al. Mutational processes shape the landscape of *TP53* mutations in human cancer. *Nat. Genet.* **50**, 1381–1387 (2018).
18. Doench, J. G. et al. Rational design of highly active sgRNAs for CRISPR–Cas9-mediated gene inactivation. *Nat. Biotechnol.* **32**, 1262–1267 (2014).
19. Sinha, S. et al. Integrated computational and experimental identification of p53, KRAS and VHL mutant selection associated with CRISPR-Cas9 editing. Preprint at *bioRxiv* https://doi.org/10.1101/407767 (2019).
20. Piras, F. et al. Lentiviral vectors escape innate sensing but trigger p53 in human hematopoietic stem and progenitor cells. *EMBO Mol. Med.* **9**, 1198–1211 (2017).
21. Zacharias, J., Romanova, L. G., Menk, J. & Philpott, N. J. p53 inhibits adeno-associated viral vector integration. *Hum. Gene Ther.* **22**, 1445–1451 (2011).

Methods

Cell culture. Descriptions of culture media used for all experiments are available in Supplementary Data 7. All cell lines were maintained at 37 °C in 5% CO_2. Cas9-expressing versions of all cell lines were generated by lentiviral transduction followed by selection with 4–10 μg ml^{-1} blasticidin (Gibco).

Cas9 transduction and transfection. Human cancer cell lines were transduced with a lentiviral vector expressing the *Streptococcus pyogenes* Cas9 nuclease under blasticidin selection (pXPR-311Cas9), and Cas9 expression was confirmed with a GFP reporter assay, as described previously[2,22,23]. For validation experiments, human cancer cell lines were transduced with a lentiviral vector expressing the *S. pyogenes* Cas9 nuclease under blasticidin selection (pLX311-Cas9) or with an empty vector control (pLX311-empty), and Cas9 expression was confirmed by western blotting. For transfection experiments, cells were transfected with 1 μg of an expression vector expressing GFP (pLX307-eGFP), Cas9 (pLX311-Cas9), or an empty vector control (pLX311-empty) using TransIT-LT1 Transfection Reagent (Mirus), per the manufacturer's protocol. After 72 h, cell lysates were collected and subjected to immunoblot analysis.

L1000 data processing. For each cell line, 16 wells of WT samples and Cas9-expressing samples were processed using the L1000 data processing pipeline, which has been described in depth elsewhere[6]. In brief, cells were transferred to 384-well plates and kept in media without additives before lysis. 384-well oligo(dT)-coated Turbocapture plates (Qiagen)were used to capture mRNA; after removing lysate and adding a Moloney murine leukemia virus (MLLV) reverse-transcription mix, the plate was washed and a mixture of both upstream and downstream probes (each containing a gene-specific sequence and a universal primer site) for each of the 978 ('landmark') genes measured was added. The probes were first annealed to complementary DNA over a 6-h period, and then ligated together to form a PCR template. After ligation, Hot Start Taq and universal primers were added to the plate, and the upstream primer was biotinylated to allow for later staining with streptavidin-phycoerythrin. Next, the PCR amplicon was hybridized to Luminex MagPlex microbeads using the complementary and probe-specific barcode on each bead; after overnight hybridization, the beads were washed and stained with streptavidin-phycoerythrin. Luminex FlexMap 3D scanners were then used to measure each bead independently, reporting bead color, identity, and fluorescence intensity of the stain. The last of these was converted into median fluorescence intensity values for each of the 978 measured genes using a deconvolution algorithm (resulting in gene expression level data). These gene expression data were then normalized relative to a set of invariant genes, and then quantile-normalized to produce QNORM level data. An inference model was applied to the QNORM data to infer gene expression changes for a total of 10,174 genes, which corresponds to the 'BING' (best inferred genes) space of genes we report above.

L1000 data quality control. All samples from the 165 unique cell lines profiled passed internal technical L1000 assay quality control measures described elsewhere[6]. In addition, all samples included passed an internal fingerprinting algorithm that verifies the identity of cell lines on L1000 plates by comparing quantile-normalized gene expression data in each well with respect to a ranked reference library of over 1,000 cell lines; samples are defined as passing if their Spearman correlation to their respective reference profile is higher than equivalent correlation values to all other reference cell line profiles.

Generation of transcriptional data dendrograms. Within each cell line (considering Cas9 and WT cells separately), the median expression value was calculated for each of the 978 directly measured genes. A dendrogram was then constructed from the aggregate of each of these signatures using Euclidean distance and complete linkage hierarchical clustering.

Generation of Cas9 transcriptional signatures. For individual Cas9 versus WT transcriptional signatures within a cell line, a signal-to-noise ratio was calculated for each of the 10,174 genes of QNORM-level data using the following formula: $\mu\times(GeneA\_Cas9-\mu\times GeneA\_WT)/(\sigma\times GeneA_{Cas9}+\sigma\times GeneA\_WT)$. When the number of samples within a class (Cas9 or WT) was below 10, the within-class standard deviation value was adjusted to $\sigma=\max(\sigma,\max(0.025\times\mu,0.025))$ to avoid zero values in the denominator. Fold change values were calculated as $\mu\times GeneA\_Cas9-\mu\times GeneA\_WT$. Meta Cas9 versus WT transcriptional signatures within each class of *TP53* mutation statuses that were considered (*TP53*-WT or *TP53*-mutant, based on the functional mutation classification reported in ref. [17]) were composed by taking the median value of the signal-to-noise ratio for each of the 10,174 genes across cell lines in the *TP53* mutation class. Aggregate Cas9 vs. WT transcriptional signatures were composed across all cell lines sharing a *TP53* mutation status by calculating a signal to noise ratio as above for each of the 10,174 genes using all samples available for all cell lines in that class.

Generation of control transcriptional signatures. To control for the possible transcriptional consequences of viral introduction, significant enrichment of pairwise Cas9 versus WT L1000 signatures was compared to enrichment values of LacZ versus WT, GFP versus WT, and empty lentiviral vector versus WT pairwise signatures. These signatures were composed from previously existing QNORM-level data by identifying untreated (hereafter referred to as WT), LacZ or GFP (hereafter referred to as control vector), and empty vector cell line samples previously used as negative controls in the L1000 US National Institutes of Health (NIH) Library of Integrated Network-based Cellular Signatures (LINCS) phase I and phase II data sets (Gene Expression Omnibus GSE92742 and GSE70138, respectively). In total, five separate cell lines (A375, HA1E, MCF7, PC3 and VCAP) had sufficient samples of good technical quality per class to compose pairwise transcriptional signatures; as these samples generally came from distinct experimental batches and clustered by project codes, batch effects were removed using the COMBAT algorithm[24]. Fifteen pairwise signatures (five empty vectors versus WT, and ten control vectors versus WT) were ultimately generated in each of the available cell lines with sufficient data, as described above.

Gene set enrichment analysis. GSEA[8] was performed using the best inferred 10,147 genes by the L1000 inference model[6]. Samples were divided into the pairwise, meta, and aggregate sets of two classes described above (in the sections 'Generation of Cas9 transcriptional signatures' and 'Generation of control transcriptional signatures') to generate several transcriptional signatures. For each signature, a ranked gene list and signal-to-noise values were used as input for the GSEA pre-ranked module of GSEA, using the Java application (version 3.0). The analysis was run using the curated 'Hallmark' signature collection from the Molecular Signature Database (MSigDB)[7]. Signatures were considered to have p53 activation if the HALLMARK_P53_PATHWAY gene set was significantly positively enriched (false discovery rate (FDR), $q<0.05$), and signatures were considered to have a DNA damage response if the HALLMARK_DNA_REPAIR gene set was significantly positively enriched (FDR, $q<0.05$).

Deep targeted sequencing. Before library preparation, DNA was fragmented (Covaris sonication) to 250 bp and further purified using Agentcourt AMPure XP beads. Size-selected DNA was ligated to sequencing adaptors with sample-specific barcodes during automated library preparation (SPRIworks, Beckman-Coulter). Libraries were pooled and sequenced on an Illumina Miseq to estimate library concentration based on the number of index reads per sample. Library construction was considered to be successful if the yield was ≥250 ng, and all samples yielded sufficient library. Normalized libraries were pooled in batches, and hybrid capture was performed using the Agilent Sureselect Hybrid Capture kit with the POPv3_824272 bait set[16]. The list of 447 genes included in POPv3_824272 is provided as Supplementary Data 3. Captures were then pooled and sequenced on one HiSeq3000 lane. Pooled sample reads were de-convoluted and sorted using the Picard tools (https://broadinstitute.github.io/picard). The reads were aligned to the reference sequence b37 edition from the Human Genome Reference Consortium using 'bwa aln' (http://bio-bwa.sourceforge.net/bwa.shtml), with the following parameters: '-q 5 -l 32 -k 2 -o 1', and duplicate reads were identified and removed using the Picard tools[25]. The alignments were further refined using the GATK tool for localized realignment around indel sites (https://software.broadinstitute.org/gatk/documentation/tooldocs/current/org_broadinstitute_gatk_tools_walkers_indels_IndelRealigner.php). Recalibration of the quality scores was also performed using GATK tools (http://gatkforums.broadinstitute.org/discussion/44/base-quality-score-recalibration-bqsr)[26,27]. Metrics for the representation of each sample in the pool were generated on the unaligned reads after sorting on the barcode (http://broadinstitute.github.io/picard/picard-metric-definitions.html). All samples achieved our target threshold of higher than 30× coverage for more than 80% of the targeted bases. The average mean exon target coverage was 283.17× (range, 92.42×–494.11×). MCF7 and A549 WT–Cas9 pairs were previously characterized[2], and analyzed together with all other cell lines. MCF7, A549 and MCF10A cell lines expressing reporter vectors and DNA barcodes were previously characterized[1], and used for the analysis presented in Extended Data Fig. 2f.

Targeted sequencing data analysis. Mutation analysis for SNVs (or point mutations) was performed using MuTect v1.1.4 (ref. [28]). Indel calling was performed using the SomaticIndelDetector tool in GATK (http://www.broadinstitute.org/cancer/cga/indelocator). Consecutive variants in the same codon were re-annotated to maximize the effect on the codon and marked as 'Phased' variants. MuTect was run in paired mode, pairing all samples to a normal sample, CEPH1408. Mutations were called if detected in > 2% of the reads (AF > 0.02). All SNVs, indels and phased variants were annotated with Variant Effect Predictor (VEP)[29]. Variants that affect protein coding regions underwent further filtering and classification based on frequency in the gnomAD, ESP and Catalogue of Somatic Mutations in Cancer (COSMIC, version 80) databases. If the frequency of the variant was more than 1% in all gnomAD and ESP populations and if the variant was not present at least twice in the COSMIC database, the variant was considered to be germline (given that no matched normal samples were available). If the frequency of the variant was more than 10% in any of the gnomAD and ESP populations, it was considered to be germline (regardless of its frequency in COSMIC). Non-silent mutations were considered to be those with the following

'Best Effect' variant classification: missense, initiator codon, nonsense, frameshift, inframe insertion or inframe deletion. Mutations that appeared more than once in COSMIC were regarded as COSMIC mutations. The complete list of variants (SNVs, indels and phased) are provided as Supplementary Data 3. *TP53* mutations were inspected manually by visualizing the sequencing BAM files in Integrative Genomics Viewer (https://software.broadinstitute.org/software/igv), and the frameshift mutation at location 17:7,579,460 in HCC1419 was updated based on this inspection. To examine the potential expansion of pre-existing inactivating mutations, we considered only somatic missense, nonsense and frameshift mutations present at $0.02 < AF < 0.48$ or $0.52 < AF < 0.98$ in the parental WT lines. To rank the genes based on the fraction of non-silent mutations out of all emerging mutations, mutations were first filtered to only those whose change in allelic fraction was at least 0.05, and genes were filtered to only those that exhibited at least 5 such mutations. Then, the proportion of non-silent mutations out of all occurring mutations was calculated for each gene.

Generation of sequencing data dendrograms. A dendrogram was constructed using complete linkage hierarchical clustering for all cell lines profiled with targeted sequencing, where Euclidean distance was calculated between vectors composed of a count value of all mutations in a given gene (if present) or zero values (for non-mutated genes in the sequencing panel) within each cell line (considering Cas9 and WT samples separately).

Pairwise detection of mutation emergence and disappearance. Mutations were determined to be acquired in Cas9 (present in Cas9 but not the WT sample of a cell line) or removed in Cas9 (present in the WT but not Cas9 sample of a cell line) at three levels of mutation-calling stringency: all mutations, non-silent mutations (variants classified as frameshifts, inframe deletions, inframe insertions, initiator codons, missense, nonsense, splice acceptors or splice donors), and mutations both in COSMIC[30] (variants with COSMIC count > 2) and with a gnomAD[31] population frequency percentage below 1% in both African-American and European populations. Within a given cell line, a given mutation in a gene was considered 'emerging' in Cas9 if its specific cDNA change was present in the Cas9 sample but not in the WT sample, and was considered 'disappearing' in Cas9 if its specific cDNA change was present in the WT sample but not in the Cas9 sample.

Dependency map data analysis. The Data Explorer tool from the DepMap portal (https://depmap.org/portal) was used to download CERES-corrected CRISPR (Public 19Q3) and RNAi dependency scores (DEMETER2, Broad) corresponding to *TP53* dependency scores in 326 cell lines with both CRISPR and RNAi annotations[32–34]. These data were fitted with a linear regression line, and then differences in residuals for *TP53*-WT versus *TP53*-mutant cell lines were compared using a one-sided Wilcoxon rank test. Dependency data were also subsetted to include only *TP53*-WT cell lines overlapping with available transcriptional data ($n = 20$ cell lines), and the same analysis of linear regression residuals was performed again, this time comparing cell lines whose transcriptional signature was positively enriched for the Hallmark p53 gene set versus cell lines without such enrichment, using a one-sided Wilcoxon rank test. To analyze the genes with significantly different dependency scores between *TP53*-WT and *TP53*-mutant cell lines, CERES-corrected CRISPR (Public 2019Q3) and RNAi (DEMETER2, Broad) dependency data were obtained from the DepMap portal and subsetted to overlapping cell lines and genes ($n = 326$ and $n = 15{,}468$, respectively). For each gene, a one-sided Wilcoxon rank test was performed comparing dependency scores in the *TP53*-WT and *TP53*-mutant lines in which scores were available for CRISPR and RNAi perturbations separately, and *P* values were corrected using the Benjamini–Hochberg (FDR) adjustment. Genes that were significantly (adjusted $P < 0.1$) more essential in *TP53*-WT than in *TP53*-mutant cell lines in the CRISPR but not (adjusted $P > 0.1$) in RNAi were determined. This gene list was subjected to a functional annotation enrichment analysis using the DAVID functional annotation tool[35], with the list of genes included in the CRISPR and RNAi screens serving as a background list.

Immunoblotting. Cells were lysed with RIPA lysis buffer (25 mM Tris-HCl at pH 7.6, 150 mM NaCl, 1% NP-40 and 0.1% SDS) and centrifuged at 15,000*g* at 4 °C for 15 min. Protein concentration was determined by the BCA assay (Novex, Life Technologies). Thirty micrograms of each sample and a PageRuler Prestained protein ladder (Thermo Scientific) were loaded on a NuPAGE 4–12% Bis-Tris gradient gel with 1× NuPAGE MOPS running buffer (Novex, Life Technologies) and separated at 150 V for 1 h. Next, a dry transfer was done at 20 V for 6 min using PVDF mini stacks in an iBlot 2 instrument (Thermo Fisher Scientific). The membrane was blocked in 5% dry milk in TBS-T for 30 min and immunoblotted overnight at 4 °C with primary antibodies against Cas9 (14697, CST), p53 (9282, CST), p21 (2947, CST), β-actin (sc-47778, Santa Cruz Biotechnology), GAPDH (5174, CST) and vinculin (V9131, Sigma-Aldrich) diluted 1:1,000 in PBS containing 5% milk. The membrane was washed in TBS-T and further incubated for 1 h with goat anti-rabbit and goat anti-mouse secondary antibodies (sc-2027 and sc-2025, Santa Cruz Biotechnology) diluted 1:10,000 in TBS-T containing 5% milk. Signal detection was performed with the SuperSignal West Femto and Pico kits (Thermo Scientific) in the ImageQuant LAS 4000 imager (GE Healthcare Life Sciences).

Real-time quantitative PCR analysis. Total RNA was extracted from cell lysates using the RNeasy Mini Kit (Qiagen). First-strand cDNA synthesis was performed with 2 mg of RNA following the M-MLV Reverse Transcriptase protocol (Thermo Fisher Scientific). In brief, samples were mixed with 250 ng random primers, 10 mM dNTPs and heated at 65 °C for 5 min. Next, 5× First-Strand Buffer (Invitrogen), 0.1 M DTT, RNaseOUT Recombinant Ribonuclease Inhibitor (40 units per ml) and M-MLV Reverse Transcriptase (200 units per ml) were added to each tube. The synthesis reaction was continued by incubation at 25 °C for 10 min, followed by 37 °C for 50 min and 70 °C for 15 min. To measure gene expression, 500 ng of cDNA were amplified in 20-ml reactions including 1× Maxima SYBR Green, 1× ROX qPCR Master Mix (Thermo Fisher Scientific) and 0.3 mM of forward and reverse primers. Primers used for the amplification of p53 transcriptional targets have been reported previously[36], using *ACTB* as an internal reference gene. Data were analyzed by the ΔΔCt method in the StepOne Software v2.1 (Thermo Fisher Scientific).

Immunofluorescence analysis. Cells were seeded in three-well slides (Electron Microscopy Science) the day before the experiment. After washing with DBPS containing Ca^{2+} (DBPS/Ca^{2+}), cells were fixed with 4% paraformaldehyde at room temperature (25 °C) for 20 min. Following washes with DBPS/Ca^{2+}, cells were permeabilized with 0.5% Triton X-100 in PBS for 10 min. Next, blocking buffer (5% BSA in TBS) was added, and slides were incubated for 1 h. For the detection of DNA damage, a primary rabbit antibody against γ-H2AX (9718, Cell Signaling Technology) was used at a 1:400 dilution. The slides were incubated for 2 h and washed in DPBS/Ca^{2+}. Next, secondary rabbit AF 488 antibody (A-21206, Thermo Fisher Scientific) and Hoechst (H3570, Thermo Fisher Scientific) for nuclei counterstaining were added at a dilution of 1:500 and 1:10,000 respectively. After incubation for 1 h, samples were washed with DPBS/$Ca^{2+}$and mounted using ProLong Diamond Antifade Mountant solution (P36970, Thermo Fisher Scientific). Slides were stored in the dark and visualized in a Revolve microscope (Echo Laboratories). Cells were scored as positive for DNA damage if > 5 foci per cell were detected for phospho-histone H2AX.

Cell competition assay. Isogenic *TP53*-WT and *TP53*-null HCT116 cell lines were purchased from Horizon. Knockout of *TP53* in these cell lines was achieved through homologous recombination of targeting vectors[9]. The status of p53 was confirmed by western blotting. *TP53*-null cells were transduced with a lentiviral vector expressing the eGFP under puromycin selection (pLX317-eGFP), and GFP expression was confirmed by flow cytometry. GFP-expressing *TP53*-null cells were mixed with *TP53*-WT cells in a 1:8 ratio, and transduced 24 h later with either Cas9 (pLX311-Cas9) or a backbone-matched control vector (pLX311-empty) under blasticidin selection. Cas9 expression was confirmed by western blotting. The ratio of green (*TP53*-null) to non-green (*TP53*-WT) cells was quantified throughout time using a CytoFLEX Flow Cytometer (Beckman Coulter). Both data acquisition and data analysis were performed on the CytoFLEX machine. A figure exemplifying the gating strategy is provided as Supplementary Figure 1.

Drug response assay. MCF7 cells were seeded at a density of 9,000 cells per well in a 96-well plate. The next day, medium was washed and fresh medium containing nutlin-3 (Sigma-Aldrich) was added to the corresponding wells in a concentration range of 0 μM–100 μM. After 72 h of incubation, levels of ATP were measured as a surrogate marker for cell viability using the CellTiter-Glo assay (Promega). Luminescence measurements were acquired in a SpectraMax reader (ATC) using an integration time of 500 ms.

Statistical analyses. The significance of the differences in transcriptional activity scores was determined by a two-tailed *t*-test. The significance of the difference in the number of enriched MSigDB Hallmark signatures between the introduction of Cas9 and that of control and empty vectors was determined by a one-sided Kolmogorov–Smirnov test. The significance of enrichment values was determined using a FDR measure[8]. The significance of the differences in the transcriptional enrichment of the p53 and the DNA repair MSigDB Hallmark signatures between *TP53*-WT and *TP53*-mutant cell lines, and between Cas9 and empty or reporter vectors, were determined by a two-tailed Fisher's exact test. The significance of the difference in p53 and p21 protein expression levels between *TP53*-WT and *TP53*-mutant cell lines, and that of the differences in the concordance between CRISPR and RNAi screens in *TP53*-WT and *TP53*-mutant cell lines, were determined by a one-tailed Wilcoxon rank test. The significance of the difference between the fraction of line showing activation following Cas9 introduction was determined by a one-tailed Fisher's exact test. The significance of the differences in mRNA levels of p53 targets between WT and Cas9 lines, and that of the difference in Cas9 activity between *TP53*-WT and *TP53*-mutant cell lines, were determined by a one-tailed *t*-test. The significance of the difference in the overall activation of p53 transcriptional targets was determined by a two-tailed one-sample *t*-test. The significance of the tendency of non-silent mutations to emerge was determined by a two-tailed one-sample Wilcoxon rank test. The significance of the differences between the number of mutations emerging in the Cas9 lines and the number of mutations disappearing in the Cas9 lines, that of the differences in the allelic fraction of pre-existing subclonal inactivating *TP53* mutations, and that of the

difference between the number of γH2AX foci, were determined by a one-tailed paired *t*-test. The significance of the expansion of *TP53* mutations in HCC1419 was determined by a binomial test, based on the allelic fraction of each mutation in the WT line. The cell line Cas9 activity levels (Supplementary Data 5) were correlated with the cell line transcriptional activity scores (as defined in ref. [6]) using a two-sided test for association using Spearman's rho. The significance of the differences in nutlin-3 sensitivity were determined using a two-way analysis of variance (ANOVA) test.

Software packages. L1000 data were analyzed using the 'cmapR' package (v1.0.1)[37]; sequencing data were analyzed using the software described above; all other data were processed and graphed using the 'tidyverse' suite of R packages (v1.2.1; https://peerj.com/preprints/3180/) and 'ggpubr' (v0.2; https://rpkgs.datanovia.com/ggpubr/index.html). Dendrograms and statistical tests were performed using the 'stats' package (v3.5.2)[38], and analyses involving R were performed using R v3.5.0 (https://cran.r-project.org/bin/windows/base/old/3.5.0/; ref. [38]). GSEA analysis was run using Java 1.8 and version 3.0 of the GSEA Java application.

Reporting Summary. Further information on research design is available in the Nature Research Reporting Summary linked to this article.

Data availability

All data sets are available within the article, its Supplementary Information, or from the corresponding authors upon request. DNA sequencing data were deposited to SRA (https://www.ncbi.nlm.nih.gov/sra) with BioProject accession number PRJNA545458. Gene expression data were uploaded to the following URL: https://clue.io/data/XPR_BASE#CAS9_BASELINE. Source Data of all immunostaining blots (in Fig. 1 and Extended Data Fig. 2) are available in the online version of this paper. Raw microscopy data are available at https://figshare.com/projects/Cas9_activates_the_p53_pathway_and_selects_for_p53-inactivating_mutations/81080.

Code availability

All of the code used to generate and/or analyze the data is publicly available.

References

22. Ben-David, U. et al. The landscape of chromosomal aberrations in breast cancer mouse models reveals driver-specific routes to tumorigenesis. *Nat. Commun.* **7**, 12160 (2016).
23. Meyers, R. M. et al. Computational correction of copy number effect improves specificity of CRISPR–Cas9 essentiality screens in cancer cells. *Nat. Genet.* **49**, 1779–1784 (2017).
24. Johnson, W. E., Li, C. & Rabinovic, A. Adjusting batch effects in microarray expression data using empirical Bayes methods. *Biostatistics* **8**, 118–127 (2007).
25. Li, H. & Durbin, R. Fast and accurate short read alignment with Burrows–Wheeler transform. *Bioinformatics* **25**, 1754–1760 (2009).
26. DePristo, M. A. et al. A framework for variation discovery and genotyping using next-generation DNA sequencing data. *Nat. Genet.* **43**, 491–498 (2011).
27. McKenna, A. et al. The Genome Analysis Toolkit: a MapReduce framework for analyzing next-generation DNA sequencing data. *Genome Res.* **20**, 1297–1303 (2010).
28. Cibulskis, K. et al. Sensitive detection of somatic point mutations in impure and heterogeneous cancer samples. *Nat. Biotechnol.* **31**, 213–219 (2013).
29. McLaren, W. et al. Deriving the consequences of genomic variants with the Ensembl API and SNP Effect Predictor. *Bioinformatics* **26**, 2069–2070 (2010).
30. Bamford, S. et al. The COSMIC (Catalogue of Somatic Mutations in Cancer) database and website. *Br. J. Cancer* **91**, 355–358 (2004).
31. Karczewski, K.J. et al. Variation across 141,456 human exomes and genomes reveals the spectrum of loss-of-function intolerance across human protein-coding genes. Preprint at *bioRxiv* https://doi.org/10.1101/531210 (2019).
32. Dempster, J.M. et al. Extracting biological insights from the Project Achilles genome-scale CRISPR screens in cancer cell lines. Preprint at *bioRxiv* https://doi.org/10.1101/720243 (2019).
33. McFarland, J. M. et al. Improved estimation of cancer dependencies from large-scale RNAi screens using model-based normalization and data integration. *Nat. Commun.* **9**, 4610 (2018).
34. Tsherniak, A. et al. Defining a cancer dependency map. *Cell* **170**, 564–576.e16 (2017).
35. Huang, D. W. et al. The DAVID Gene Functional Classification Tool: a novel biological module-centric algorithm to functionally analyze large gene lists. *Genome Biol.* **8**, R183 (2007).
36. Kung, C. P., Khaku, S., Jennis, M., Zhou, Y. & Murphy, M. E. Identification of TRIML2, a novel p53 target, that enhances p53 SUMOylation and regulates the transactivation of proapoptotic genes. *Mol. Cancer Res.* **13**, 250–262 (2015).
37. Enache, O. M. et al. The GCTx format and cmap{Py, R, M, J} packages: resources for optimized storage and integrated traversal of annotated dense matrices. *Bioinformatics* **35**, 1427–1429 (2019).
38. R Development Core Team. *R: A Language and Environment for Statistical Computing* (R Foundation for Statistical Computing, 2010).

Acknowledgements

We thank A. Subramanian, D. Root, T. Natoli, C. Kadoch, S. Cassel and C. Collings for helpful discussions; X. Lu, A. Giacomelli, K. Labella, K. Sanson and W. Hahn for contributing reagents; M. Ducar and S. Drinan for assistance with the OncoPanel assay; and F. Piccioni for assistance with Cas9 cell line generation. This work was supported by the NIH (R01 CA18828, CA215489 and CA219943 to R.B.), the Gray Matters Brain Cancer Foundation (R.B.), Pediatric Brain Tumor Foundation (R.B.), HHMI (T.R.G.) and HFSP (U.B.-D.). Research in the the laboratory of U.B.-D. is supported by the Azrieli Foundation, the Richard Eimert Research Fund on Solid Tumors, the Tel-Aviv University Cancer Biology Research Center, and the Israel Cancer Association.

Author contributions

U.B.-D. conceived and supervised the project; O.M.E. and U.B.-D. collected the data and performed the computational analyses; V.R., M.A. and U.B.-D. carried out the experiments; D.L. and D.D. assisted with the L1000 assay; S.P. and N.C. assisted with western blots; J.H. assisted with the mutation data analysis; S.P., J.G.D. and F.V. contributed the matched parental and Cas9-expressing cell lines; A.N. and A.T. assisted with the Oncopanel assay and analysis. O.M.E., V.R., R.B., T.R.G. and U.B.-D. analyzed the data and wrote the manuscript. R.B., T.R.G. and U.B.-D. directed the project.

Competing interests

J.G.D. consults for Tango Therapeutics, Foghorn Therapeutics, and Pfizer. T.R.G. is a paid advisor to GlaxoSmithKline and Sherlock Biosciences. R.B. owns shares in Ampressa and receives grant funding from Novartis. D.D. is an employee of Cellarity.

Additional information

Extended data is available for this paper at https://doi.org/10.1038/s41588-020-0623-4.

Supplementary information is available for this paper at https://doi.org/10.1038/s41588-020-0623-4.

Correspondence and requests for materials should be addressed to U.B.-D.

Reprints and permissions information is available at www.nature.com/reprints.

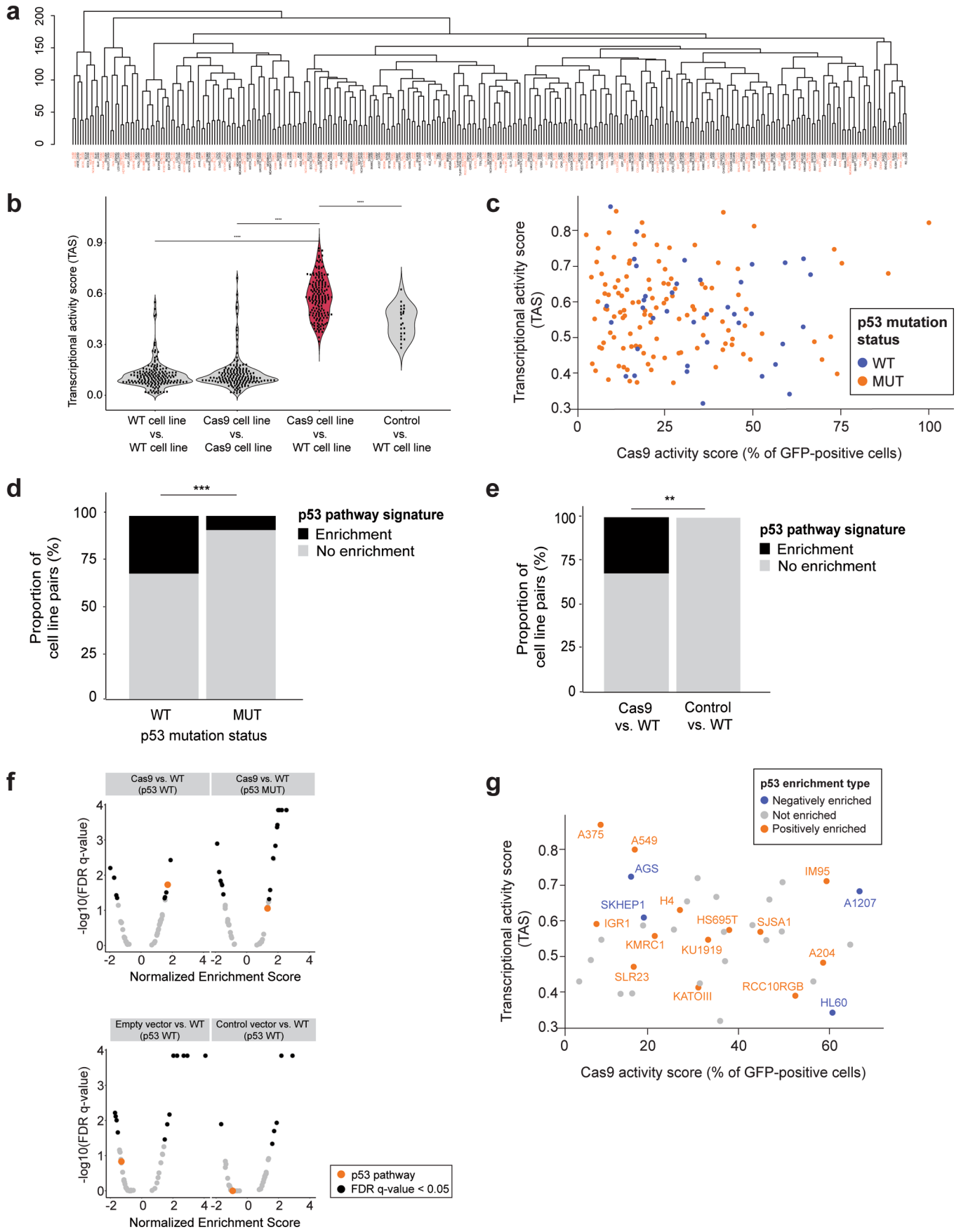

Extended Data Fig. 1 | See next page for caption.

Extended Data Fig. 1 | Cas9 introduction activates the p53 pathway (related to Fig. 1). a, Unsupervised hierarchical clustering of 165 WT/Cas9 cell line pairs, based on their median L1000 transcriptional profiles (landmark space, n = 978 genes). Cell line pairs are colored in red and black, alternately, to highlight that all Cas9 lines cluster together with their parental WT lines. **b**, Transcriptional activity scores (TAS)[6] comparison of technical replicates of 165 parental lines, 165 technical replicates of Cas9 lines, 165 Cas9 lines vs. parental lines, or 22 control vector lines vs. parental cell lines. *, $P < 2 \times 10^{-16}$, $P < 2 \times 10^{-16}$ and $P = 2.5 \times 10^{-7}$, two-tailed paired *t* test. Data points represent cell line pairs. **c**, Lack of correlation between Cas9 activity levels (measured by GFP levels; see Online Methods) and the strength of the transcriptional response (measured by TAS). $P = 0.68$, two-tailed test for association using Spearman's *rho*. 158 lines are colored by their *TP53* mutation status; 7 lines excluded due to lack of Cas9 activity data. **d**, The proportion of lines (n = 165) with an activated p53 pathway activity following Cas9 introduction, in *TP53*-WT vs. *TP53*-mutant cell lines. *, $P = 0.0007$, two-tailed Fisher's exact Test. **e**, The proportion of *TP53*-WT lines (n = 61) with an activated p53 pathway activity following Cas9 or empty/reporter vector introduction. *, $P = 0.006$, two-tailed Fisher's exact Test. **f**, The degree and significance of enrichment of the 50 MSigDB Hallmark biological pathways, following the introduction of empty vectors, reporter vectors and Cas9 into *TP53*-WT cell lines, and the introduction of Cas9 into *TP53*-mutant cell lines. Black, significantly enriched (GSEA enrichment score with multiple hypotheses correction; $q < 0.05$) pathways. Orange, the p53 pathway. Each plot represents the results of one Meta expression signature (see Online Methods). **g**, Comparison of Cas9 activity levels and TAS, as in (**d**), but only 40 available *TP53*-WT lines are presented. Cell lines are colored by whether their gene expression profiles were enriched for the p53 Hallmark gene set (and in which direction). $P = 0.30$, two-tailed test for association using Spearman's *rho*.

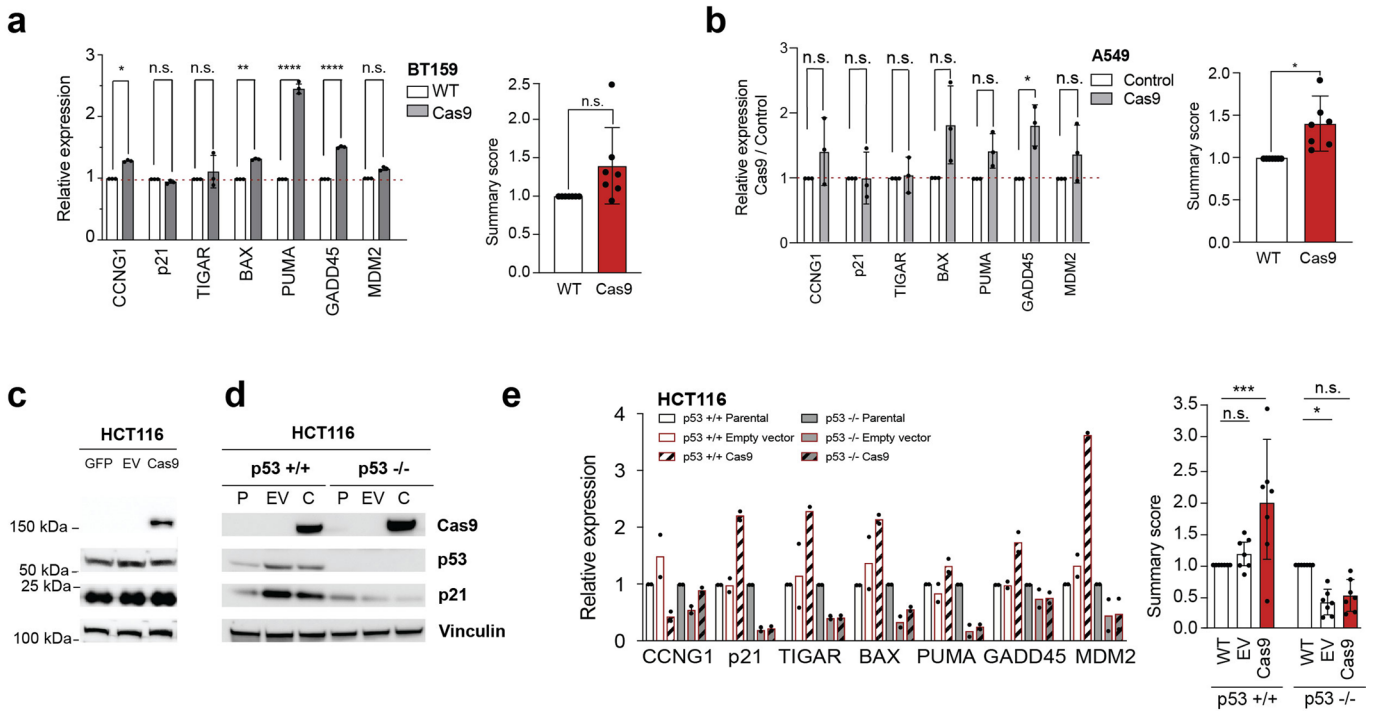

Extended Data Fig. 2 | Confirmation of p53 activation following Cas9 introduction (related to Fig. 1). a, Left: confirmation of p53 pathway activation in BT159 cell lines by RT-qPCR analysis of 7 transcriptional targets of p53. *, $P = 0.017$, **, $P = 0.0065$, ****, $P < 0.0001$, one-tailed *t* test. Data values represent the means of 3 replicates, with error bars corresponding to S.D. Right: the average activation of p53 transcriptional targets. $P = 0.08$, two-tailed one-sample *t* test. Data values represent the means of the 7 targets, with error bars corresponding to S.D. **b**, Left: RT-qPCR analysis of 7 transcriptional targets of p53 in A549 (*TP53*-WT) before and after its transduction with Cas9 or with three control vectors: luciferase, GFP or DNA barcode. *, $P = 0.048$, one-tailed *t* test. Data values represent the means of the 3 control vectors and of 3 biological replicates of Cas9, with error bars corresponding to S.D. Right: the average activation of p53 transcriptional targets. *, $P < 0.05$, two-tailed one-sample *t* test. Data values represent the means of the 7 targets, with error bars corresponding to S.D. **c**, Protein levels of Cas9, p53, p21 and a housekeeping protein in HCT116 cells transfected with GFP, Cas9 or a backbone-matched empty vector (EV). Results represent a single experiment. **d**, Protein levels of Cas9, p53, p21 and a housekeeping protein in isogenic *TP53*-WT (P) and *TP53*-null HCT116 cells before and after transduction of Cas9 (C) or of a backbone-matched control vector (EV). Results represent a single experiment. **e**, Left: RT-qPCR analysis of 7 transcriptional targets of p53 shows p53 pathway activation specifically in the Cas9-expressing *TP53*-WT HCT116 cells. Data values represent the means of 2 replicates, with error bars corresponding to S.D. Right: the average activation of p53 transcriptional targets. *, $P = 0.028$, ***, $P = 0.0004$, ****, $P < 0.0001$, two-tailed one-sample *t* test. Data values represent the means of the 7 targets, with error bars corresponding to S.D.

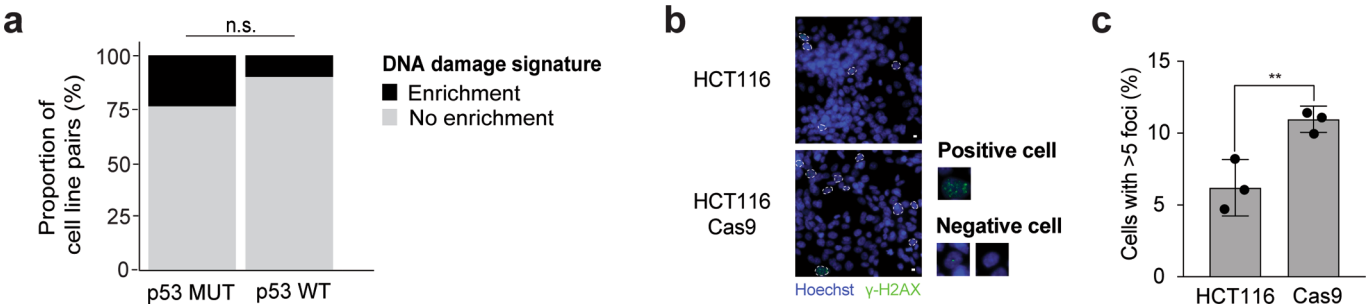

Extended Data Fig. 3 | Cas9 introduction activates the DNA damage response (related to Fig. 2). a, The proportion of cell lines (n = 165) with a positively enriched DNA damage transcriptional signature, following Cas9 introduction. *, $P = 0.07$; two-tailed Fisher's exact Test. **b**, Fluorescent microscopy images of γH2AX foci (green) and DAPI (blue) in parental *TP53*-WT HCT116 cells and following Cas9 transduction. Cells with > 5 foci have been marked in white. Scale bar represents 10 μm. **c**, Quantification of γH2AX foci from three independent repeats; n = 1,765 and n = 2,523, for WT and Cas9 HCT116 cells, respectively. **, $P = 0.0095$; one-tailed *t* test. Data show means, with error bars corresponding to S.D.

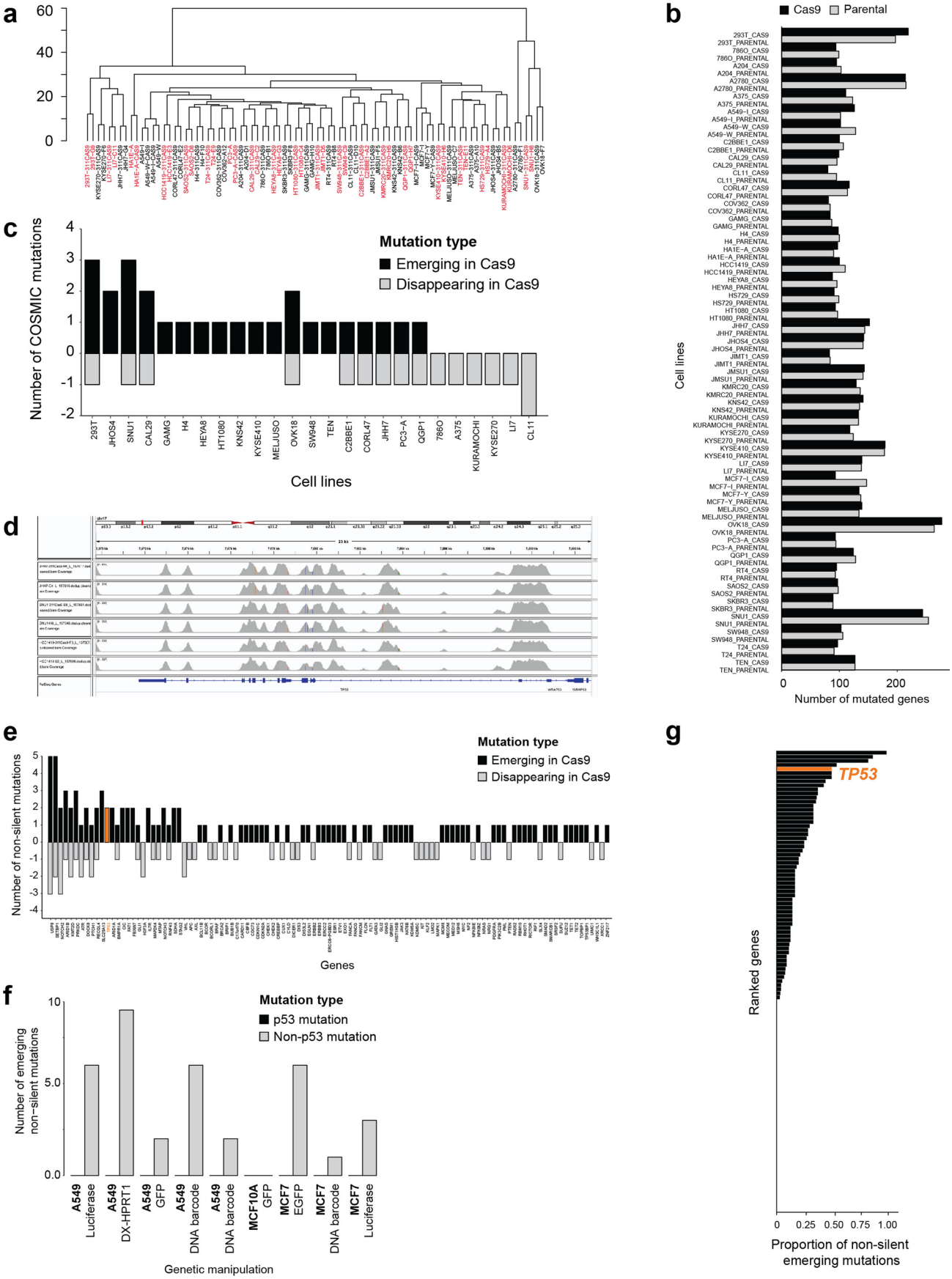

Extended Data Fig. 4 | See next page for caption.

Extended Data Fig. 4 | Cas9 introduction selects for inactivating TP53 mutations (related to Fig. 3). a, Unsupervised hierarchical clustering of 42 WT/Cas9 cell line pairs across 40 independent cell lines, based on their genetic profiles. Cell line pairs are colored in red and black, alternately, to highlight that all Cas9 lines cluster together with their parental WT lines. **b**, The count of overall mutations detected across the 42 WT/Cas9 cell line pairs. **c**, The number of recurrent COSMIC mutations that differ between the Cas9 lines and their matched WT lines (that is, detected either in the parental or in the Cas9 line, but not in both). Emerging mutations are shown in black, disappearing mutations in gray, for the 25 cell lines with any COSMIC mutations present. *, $P = 0.027$, one-tailed paired *t* test. **d**, Sequencing coverage of the *TP53* exons in the three cell line pairs in which emergence or expansion of *TP53* mutations were detected. **e**, Cancer genes ranked by their tendency to acquire mutations in the Cas9 lines. Emerging mutations are shown in black, disappearing mutations in gray. *TP53* is highlighted in orange. **f**, The number of non-silent mutations that differ between WT lines and their reported or barcoded derivatives. No mutation in TP53 was observed in 9 independent experiments across three *TP53*-WT cell lines. **g**, Cancer genes ranked by the proportion of silent mutations out of all emerging (silent and non-silent) mutations. *TP53* is highlighted in orange, and is among the top ~1% of genes (out of 128 genes with a non-silent mutation present).

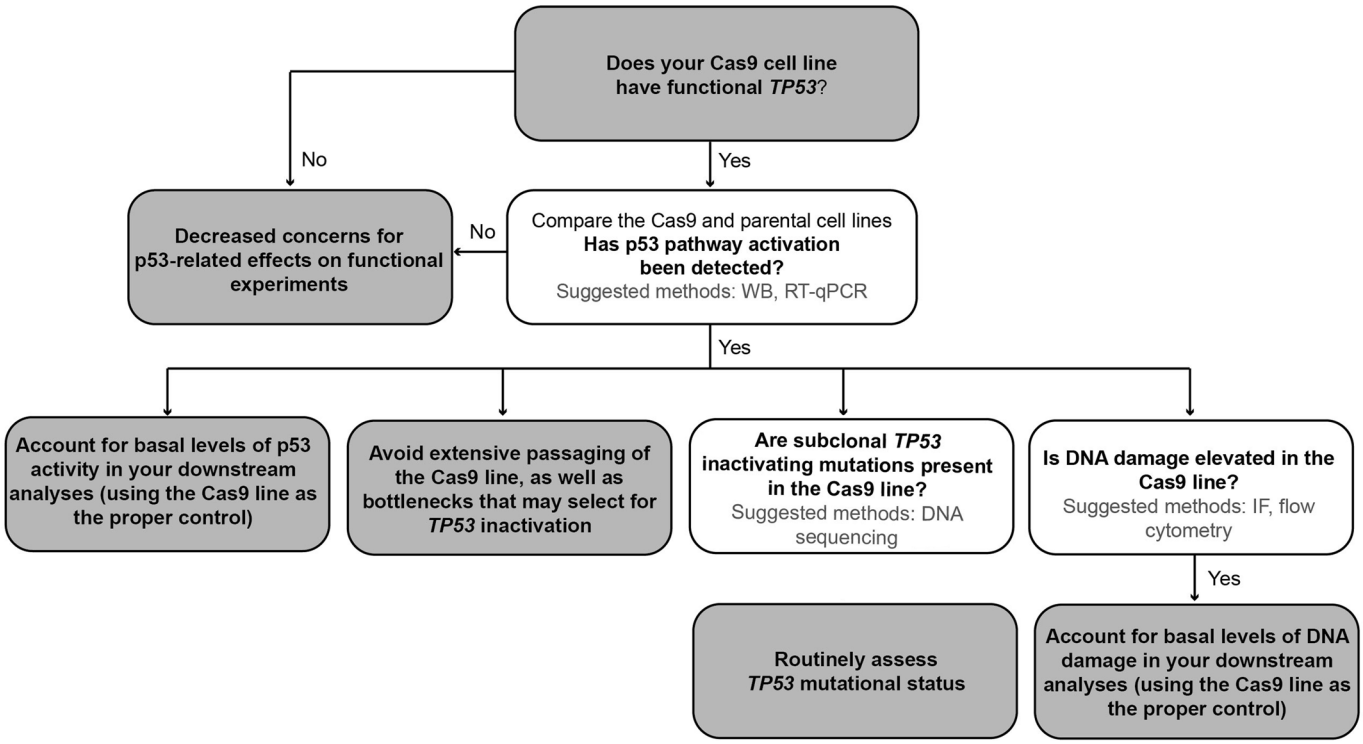

Extended Data Fig. 5 | Proposed workflow for Cas9-related laboratory experiments. When conducting systematic CRISPR/Cas9-mediated screens or focused studies in *TP53*-WT cancer cell lines, we recommend determining the basal activation level of the p53 pathway in the Cas9-expressing line. If there is p53 activation, it is recommended to assess Cas9-derived ongoing DNA damage accumulation as well. Finally, as continuous Cas9 expression poses a selection pressure that over time may be reflected in the emergence or expansion of p53-inactivating mutations, it is recommended to avoid extensive passaging and culture bottlenecks that may accelerate this process.

nature research

Corresponding author(s): Uri Ben-David

Last updated by author(s): February 5, 2020

Reporting Summary

Nature Research wishes to improve the reproducibility of the work that we publish. This form provides structure for consistency and transparency in reporting. For further information on Nature Research policies, see Authors & Referees and the Editorial Policy Checklist.

Statistics

For all statistical analyses, confirm that the following items are present in the figure legend, table legend, main text, or Methods section.

n/a	Confirmed	
☐	☒	The exact sample size (*n*) for each experimental group/condition, given as a discrete number and unit of measurement
☐	☒	A statement on whether measurements were taken from distinct samples or whether the same sample was measured repeatedly
☐	☒	The statistical test(s) used AND whether they are one- or two-sided *Only common tests should be described solely by name; describe more complex techniques in the Methods section.*
☐	☒	A description of all covariates tested
☐	☒	A description of any assumptions or corrections, such as tests of normality and adjustment for multiple comparisons
☐	☒	A full description of the statistical parameters including central tendency (e.g. means) or other basic estimates (e.g. regression coefficient) AND variation (e.g. standard deviation) or associated estimates of uncertainty (e.g. confidence intervals)
☐	☒	For null hypothesis testing, the test statistic (e.g. *F*, *t*, *r*) with confidence intervals, effect sizes, degrees of freedom and *P* value noted *Give P values as exact values whenever suitable.*
☒	☐	For Bayesian analysis, information on the choice of priors and Markov chain Monte Carlo settings
☒	☐	For hierarchical and complex designs, identification of the appropriate level for tests and full reporting of outcomes
☒	☐	Estimates of effect sizes (e.g. Cohen's *d*, Pearson's *r*), indicating how they were calculated

Our web collection on statistics for biologists contains articles on many of the points above.

Software and code

Policy information about availability of computer code

Data collection	All software used in data collection were published , and are described in the Methods section of the paper. No commercial SW were used. Sequencing alignment: Pooled sample reads were de-convoluted and sorted using the Picard tools release 2.14 (http://broadinstitute.github.io/picard). Alignments were refined using the GATK tool (R4.beta.3) for localized realignment around indel sites (https://software.broadinstitute.org/gatk/documentation/tooldocs/current/org_broadinstitute_gatk_tools_walkers_indels_IndelRealigner.php). Recalibration of the quality scores was also performed using GATK tools (R4.beta.3) (http://gatkforums.broadinstitute.org/discussion/44/base-quality-score-recalibration-bqsr).
Data analysis	All software used in the analysis were published , and are described in the Methods section of the paper. No commercial SW were used. L1000 data were analyzed using the 'cmapR' package (v1.0.1)32; all other data were processed and graphed using the 'tidyverse' suite of R packages (v1.2.1; https://peerj.com/preprints/3180/) and 'ggpubr' (v0.2; https://rpkgs.datanovia.com/ggpubr/index.html). Dendrograms and statistical tests were performed using the 'stats' package (v3.5.2)33, and analyses involving R were performed using R v3.5.033. GSEA analysis was run using Java 1.8 and version 3.0 of the GSEA Java application. Sequencing data analysis: Mutation analysis for single nucleotide variants (point mutations, or SNVs) was performed using MuTect v1.1.4. Indel calling was performed using the SomaticIndelDetector tool in GATK R4.beta.3 (http://www.broadinstitute.org/cancer/cga/indelocator). Manual inspection of BAM files was done using the Integrative Genomics Viewer v2.6.0 (https://software.broadinstitute.org/software/igv).

For manuscripts utilizing custom algorithms or software that are central to the research but not yet described in published literature, software must be made available to editors/reviewers. We strongly encourage code deposition in a community repository (e.g. GitHub). See the Nature Research guidelines for submitting code & software for further information.

Data

Policy information about availability of data

All manuscripts must include a data availability statement. This statement should provide the following information, where applicable:

- Accession codes, unique identifiers, or web links for publicly available datasets
- A list of figures that have associated raw data
- A description of any restrictions on data availability

All datasets are available within the article, its Supplementary Information, or from the corresponding authors upon request. DNA sequencing data were deposited to SRA with BioProject accession number PRJNA545458. Gene expression data were uploaded to the following URL: https://clue.io/data/XPR_BASE#CAS9_BASELINE. Source Data of all immunostaining blots will be available in the online version of this paper.

Field-specific reporting

Please select the one below that is the best fit for your research. If you are not sure, read the appropriate sections before making your selection.

☒ Life sciences ☐ Behavioural & social sciences ☐ Ecological, evolutionary & environmental sciences

For a reference copy of the document with all sections, see nature.com/documents/nr-reporting-summary-flat.pdf

Life sciences study design

All studies must disclose on these points even when the disclosure is negative.

Sample size	We collected as many pairs of parental-Cas9 cell lines as we could obtain. For each analysis, all available cell lines were used. Post-hoc power calculations of parametric tests performed showed that our sample size was sufficient to identify gene expression changes corresponding to at least moderate effect sizes (computed using Cohen's D or Hedge's G; power >80% for Fig. ED1B,D,E) and shifts in mutation status corresponding to at least moderate effect sizes (computed using Cohen's D or Hedge's G; power > 80% for Fig. 3A and Fig. ED4C).
Data exclusions	Samples with low quality DNA or RNA were excluded from the genetic and transcriptional profiling. Quality control was performed both for the genetic and for the transactional analyses based on pre-determined established thresholds (described in the Methods section). Only samples that passed these pre-determined thresholds QC were further analyzed.
Replication	The DNA analysis was performed with one technical replicate per biological sample. The RNA analysis was performed with 5 technical replicates per biological sample. qPCR analyses were performed with three technical replications per biological sample. Western blotting was performed at least twice per biological sample. The experimental findings were reliably reproduced.
Randomization	No randomization was done, as all available cell lines were used (therefore, randomization was not required).
Blinding	Genetic and transcriptional profiling were performed without the investigators' knowledge of each sample identity. Investigators were not blind to sample identity during the in vitro experiments because cell lines required different culture conditions.

Reporting for specific materials, systems and methods

We require information from authors about some types of materials, experimental systems and methods used in many studies. Here, indicate whether each material, system or method listed is relevant to your study. If you are not sure if a list item applies to your research, read the appropriate section before selecting a response.

Materials & experimental systems

n/a	Involved in the study
☐	☒ Antibodies
☐	☒ Eukaryotic cell lines
☒	☐ Palaeontology
☒	☐ Animals and other organisms
☒	☐ Human research participants
☒	☐ Clinical data

Methods

n/a	Involved in the study
☒	☐ ChIP-seq
☐	☒ Flow cytometry
☒	☐ MRI-based neuroimaging

Antibodies

Antibodies used	For WB, the following primary antibodies were used: Cas9 (#14697, CST, mouse monoclonal, 1:1000) p53 (#9282, CST, rabbit polyclonal, 1:1000) p21 (#2947, CST, rabbit monoclonal, 1:1000) β-Actin (sc-47778, Santa Cruz Biotechnology, mouse monoclonal, 1:1000)

GAPDH (#5174, CST, rabbit polyclonal, 1:1000)
Vinculin (V9131, Sigma-Aldrich, mouse monoclonal, 1:1000)
The secondary antibodies that were used were:
Normal rabbit IgG (sc-2027, Santa Cruz Biotechnology, 1:10000)
Normal mouse IgG (sc-2025, Santa Cruz Biotechnology, 1:10000)
For the detection of DNA damage, a primary rabbit monoclonal antibody
against γ-H2AX (#9718, Cell Signaling Technology, 1:400) was used, followed by a secondary rabbit AF 488 antibody (A-21206, Thermo Fisher Scientific, donkey polyclonal, 1:500)

Validation

Antibodies were selected based on their use in the literature in human cancer cell lines, and previous experience of the investigators. Full antibody information is provided in the Methods section of the paper. Positive and negative controls were used in all experiments including antibodies.

Product citations (n):
Cas9 (n = 13, https://www.cellsignal.com/products/primary-antibodies/cas9-7a9-3a3-mouse-mab/14697)
p53 (n = 296, https://www.cellsignal.com/products/primary-antibodies/p53-antibody/9282)
p21 (n = 684, https://www.cellsignal.com/products/primary-antibodies/p21-waf1-cip1-12d1-rabbit-mab/2947)
β-Actin (n = 7939, https://www.scbt.com/p/beta-actin-antibody-c4)
GAPDH (n = 792, https://www.sigmaaldrich.com/catalog/product/sigma/g9545?lang=en&region=US)
Vinculin (n = 721, https://www.sigmaaldrich.com/catalog/product/sigma/v9131?lang=en&region=US)
Mouse (n = 2080, https://www.scbt.com/p/normal-mouse-igg)
Rabbit (n = 17 select product citations in data sheet)
γ-H2AX (n = 623, https://www.cellsignal.com/products/primary-antibodies/phospho-histone-h2a-x-ser139-20e3-rabbit-mab/9718)
rabbit AF 488 (n = 70, https://www.thermofisher.com/antibody/product/Donkey-anti-Rabbit-IgG-H-L-Highly-Cross-Adsorbed-Secondary-Antibody-Polyclonal/A-21206)

Eukaryotic cell lines

Policy information about cell lines

Cell line source(s)

Established widely-used human cancer cell lines were used in this study (detailed in Supplementary Data 7):
293T
42MGBA
786O
8305C
8MGBA
A1207
A204
A253
A2780
A375
A549
AGS
AM38
AN3CA
AU565
BC3C
BICR16
BICR56
BICR6
BL41
BT159
BT549
C2BBE1
CAL29
CAL33
CAL78
CALU6
CAMA1
CAS1
CHAGOK1
CL11
CL14
COLO792
COLO800
CORL279
CORL47
COV362
COV504
DKMG
DND41
DU145
ECC10

EFE184
EFM-192A
EN
ES2
ESS1
F36P
FADU
FU97
GAMG
GCT
GI1
GMS10
GSU
H4
HA1E
HARA
HCC1187
HCC1395
HCC1419
HCC1428
HCC1954
HCT116
HEC151
HEC1B
HEC6
HEL9217
HEP3B217
HEYA8
HL60
HS578T
HS695T
HS729
HT1080
HT29
IGR1
IGR39
IM95
ISTMES2
JHH4
JHH5
JHH7
JHOS4
JIMT1
JMSU1
KATOIII
KLE
KMBC2
KMRC1
KMRC20
KMS34
KNS42
KS1
KU1919
KURAMOCHI
KYSE140
KYSE270
KYSE410
LI7
LOVO
LUDLU1
M059K
MCF10A
MCF7
MDAMB231
MDAMB415
MDAMB436
MDAMB453
MELJUSO
MFE280
MFE319
NCIH1048
NCIH1155
NCIH1568
NCIH1573
NCIH2066

NCIH2172
NCIH2196
NCIH2882
NCIH526
NCIH647
NCIH838
NCIN87
NMCG1
ONCODG1
OSRC2
OV7
OV90
OVCAR5
OVK18
OVTOKO
PC3
PK1KLM1
PLCPRF5
QGP1
RCC10RGB
RCM1
RD
RH41
RKN
RT4
SAOS2
SCC25
SCC4
SF126
SF172
SF268
SF295
SHP77
SJSA1
SKBR3
SKHEP1
SKNDZ
SKUT1
SLR20
SLR23
SNGM
SNU1
SNU1077
SNU1079
SNU119
SNU201
SNU216
SNU387
SNU398
SNU423
SNU466
SNU475
SNU840
SNU878
SNU886
SUIT2
SW1710
SW48
SW948
SW982
T24
T98G
TCCSUP
TE11
TE5
TE6
TEN
TM31
TUHR14TKB
U251MG
UACC812
UMUC3
VMCUB1
WM1799
WM2664

	YAPC YD8 YKG1 ZR7530 The source of all cell lines is the Cancer Cell Line Encyclopedia, except for the HCT116 isogenic strains (purchased from Horizon Discovery), MCF10A (purchased from Horizon Discovery) and BT159 (a gift from Prof. Ligon's lab at Dana-Farber Cancer Institute)
Authentication	Cell line authentication was performed using SNP-based DNA fingerprinting.
Mycoplasma contamination	Cell lines were tested negative for mycoplasma contamination using a Lonza kit.
Commonly misidentified lines (See ICLAC register)	Cell lines are not in the list of misidentified cell lines.

Flow Cytometry

Plots

Confirm that:

☒ The axis labels state the marker and fluorochrome used (e.g. CD4-FITC).

☒ The axis scales are clearly visible. Include numbers along axes only for bottom left plot of group (a 'group' is an analysis of identical markers).

☒ All plots are contour plots with outliers or pseudocolor plots.

☒ A numerical value for number of cells or percentage (with statistics) is provided.

Methodology

Sample preparation	Isogenic TP53-WT/null, ARID1A-WT/null and FBWX1-WT/null HCT116 cell lines were used. p53 expression status was confirmed by western blotting. The mutatnt cell lines were transduced with a lentiviral vector expressing EGFP under puromycin selection (pLX317-eGFP), and GFP expression was confirmed. GFP-expressing cells were mixed with their corresponding WT cells in a 1:8 ratio, and transduced 24 hr later with either Cas9 (pLX311-Cas9) or a backbone-matched control vector (pLX311-empty) under blasticidin selection. Cas9 expression was confirmed by western blotting. The ratio of green (mutatnt) to non-green (WT) cells was quantified throughout time.
Instrument	CytoFLEX Flow Cytometer (Beckman Coulter)
Software	Both data acquisition and data analysis were performed on the CytoFLEX machine
Cell population abundance	No sorting was performed.
Gating strategy	A preliminary SSC-A/FSC-A gate was determined to exclude cell debris, and a FSC-A/FSC-H gate was then determined to exclude doublets. GFP positivity threshold was defined in each experiment using negative and positive control populations (i.e., the non-mixed populations).

☒ Tick this box to confirm that a figure exemplifying the gating strategy is provided in the Supplementary Information.